J. Math. Anal. Appl. 483 (2020) 123577

Contents lists available at ScienceDirect

Journal of Mathematical Analysis and Applications

www.elsevier.com/locate/jmaa

Oscillations in a cAMP signalling model for cell aggregation – a geometric analysis

Zhouqian Miao [a], Nikola Popović [b,*], Peter Szmolyan [a]

[a] *Technische Universität Wien, Institute for Analysis and Scientific Computing, Wiedner Hauptstraße 8-10, 1040 Wien, Austria*
[b] *University of Edinburgh, School of Mathematics and Maxwell Institute for Mathematical Sciences, James Clerk Maxwell Building, King's Buildings, Peter Guthrie Tait Road, Edinburgh EH9 3FD, United Kingdom*

ARTICLE INFO

Article history:
Received 10 May 2019
Available online 11 October 2019
Submitted by J. Shi

Keywords:
cAMP signalling
Singular perturbation
Geometric singular perturbation theory
Blow-up technique
Relaxation oscillation
Periodic orbit

ABSTRACT

We study a singularly perturbed model for a cyclic adenosine monophosphate (cAMP) signalling system that controls aggregation of the amoeboid microorganism *Dictyostelium discoideum*. The model, which is based on a classical model due to Martiel and Goldbeter [16], takes the form of a planar system of ordinary differential equations with two singular perturbation parameters which manifest very differently: while one parameter encodes the separation of scales between the slow and fast variables, the other induces a non-uniformity in the corresponding vector field in the singular limit. We apply geometric singular perturbation theory and the desingularisation technique known as "blow-up" to construct a family of attracting, periodic (relaxation-type) orbits; in the process, we elucidate the novel singular structure of the model, and we describe in detail the resulting oscillatory dynamics.

1. Introduction

In the present article, we perform a geometric analysis of a singularly perturbed model for a cyclic adenosine monophosphate (cAMP) signalling system that controls aggregation of the amoeboid microorganism *Dictyostelium discoideum*. The periodic synthesis of pulses of cAMP constitutes an example of a biochemical oscillation of clear physiological significance [8]. Two main types of dynamics are observed in cAMP signalling systems: autonomous oscillation [5,8,7] and relay of super-threshold pulses [19,22]. The model of cAMP signalling due to Goldbeter and Segel [9,10] shows that both types are caused by the auto-catalytic regulation of adenylate cyclase, the latter enzyme being activated on the binding of extracellular cAMP to the cell receptor [18,6]. Moreover, relay behaviour has been linked to autonomous oscillation, which

* Corresponding author.
E-mail address: nikola.popovic@ed.ac.uk (N. Popović).

https://doi.org/10.1016/j.jmaa.2019.123577
0022-247X/

represents the excitability of the system. In the model by Goldbeter and Segel, the substrate adenosine triphosphate (ATP) plays a role in the oscillation and relay response; however, it has been shown experimentally that intracellular ATP remains constant during the oscillation [20], and that the relay results from the absence of ATP consumption when the cAMP receptor is uncoupled from adenylate cyclase upon incubation with caffeine [24]. These observations were made under the assumption that adenylate cyclase is an allosteric enzyme; moreover, significant variation is required in the concentration of ATP. Martiel and Goldbeter [16] considered another situation, whereby the mechanism is based on desensitisation of the cAMP receptor to extracellular cAMP. The full model proposed in [16], which consists of seven differential equations, can be reduced to the three-variable system

$$\frac{d\rho_T}{dt} = -f_1(\gamma)\rho_T - f_2(\gamma)(1-\rho_T), \tag{1a}$$

$$\frac{d\beta}{dt} = q\sigma\phi(\rho_T,\gamma) - (k_i+k_t)\beta, \tag{1b}$$

$$\frac{d\gamma}{dt} = \frac{k_t}{h}\beta - k_e\gamma, \tag{1c}$$

with

$$f_1(\gamma) = \frac{k_1+k_2\gamma}{1+\gamma}, \quad f_2(\gamma) = \frac{k_1L_1+k_2L_2\gamma}{1+c\gamma}, \tag{2a}$$

$$\phi(\rho_T,\gamma) = \frac{\alpha(\lambda\theta+\epsilon Y^2)}{1+\alpha\theta+\epsilon Y^2(1+\alpha)}, \quad \text{and} \quad Y = \frac{\rho_T\gamma}{1+\gamma}. \tag{2b}$$

Here, ρ_T represents the total fraction of receptor in the active state, while β and γ denote intracellular and extracellular concentrations, respectively, of cAMP. Moreover, c, α, λ, θ, ϵ, σ, h, k_i, k_t, k_e, k_j, L_j $(j=1,2)$, and q are suitably defined parameters; details can be found in [16]. Equation (1) can be reduced further to a two-variable system for sufficiently large values of the parameters q, k_i, and k_t, which allows for a quasi-steady-state assumption to be made for β: Equation (1b) implies $\beta = q\sigma\frac{\phi(\rho_T,\gamma)}{(k_i+k_t)}$. Therefore, the effective dynamics is then characterised by the following planar system of nonlinear ordinary differential equations (ODEs),

$$\frac{d\rho_T}{dt} = -f_1(\gamma)\rho_T - f_2(\gamma)(1-\rho_T), \tag{3a}$$

$$\frac{d\gamma}{dt} = \frac{q\sigma k_t}{h(k_i+k_t)}\phi(\rho_T,\gamma) - k_e\gamma. \tag{3b}$$

While experiments [16] indicate that $q \gg 1$, whereas k_i and k_t are of the order $\mathcal{O}(1)$, and hence lower than what is expected for a quasi-steady-state assumption, numerical simulation shows that the planar system in (3) provides a reasonably good approximation for the three-variable system in (1). Therefore, (3) can be considered as the core mechanism in the cAMP signalling system, allowing for a phase plane analysis of relay and oscillation due to the simplicity of the governing equations.

With these observations in mind, we now introduce the singular perturbation problem considered in the present article, which is based on the three-variable Martiel-Goldbeter model, Equation (1), in the scaling of Lițcanu and Velázquez [15]:

$$R_\tau = \kappa(U+\mathcal{P}\varepsilon)\frac{\mu(U+\varepsilon)-(U+d\varepsilon)R}{(U+\frac{\varepsilon}{c})(U+\varepsilon)}, \tag{4a}$$

$$W_\tau = \frac{b\varepsilon(U+\varepsilon)^2+\Theta R^2U^2}{(U+\varepsilon)^2+\Lambda R^2U^2} - W, \tag{4b}$$

$$U_\tau = \Gamma(W - U). \tag{4c}$$

The state variables, which are now denoted by R, W, and U, correspond to the total proportion of receptors in the active state ρ_T, the concentration of intracellular cAMP β, and the concentration of extracellular cAMP γ, respectively; the model parameters are defined in Table 1, with $\tau = (k_i + k_t)t$.

Imposing a quasi-steady-state assumption, as was done for (1) above, we find $W = U$, thus reducing the model to the two-variable system

$$R_\tau = \kappa(U + \mathcal{P}\varepsilon)\frac{\mu(U+\varepsilon) - (U + d\varepsilon)R}{(U + \frac{\varepsilon}{c})(U+\varepsilon)}, \tag{5a}$$

$$U_\tau = \frac{b\varepsilon(U+\varepsilon)^2 + \Theta R^2U^2}{(U+\varepsilon)^2 + \Lambda R^2U^2} - U. \tag{5b}$$

Given the definition of the parameters κ and ε in [15], which are both assumed to be small, (5) is singularly perturbed ("slow-fast"). Here, we emphasise that the impact of these two parameters on the dynamics of (5) manifests very differently: while the parameter κ is a "conventional" singular perturbation parameter that reflects the separation of scales between the slow variable R and the fast variable U, the parameter ε induces a different type of singular perturbation which is reflected by the non-uniformity of the limit as $\varepsilon \to 0$ in Equation (5); specifically, that limit will depend fundamentally on whether $U \gg \varepsilon$ or $U = \mathcal{O}(\varepsilon)$ therein. Correspondingly, the limit as $\kappa \to 0$ in Equation (5) can be studied using Fenichel's geometric singular perturbation theory [4], while the structure of the resulting asymptotics in ε can be resolved rigorously via the blow-up technique [3]. In particular, geometric singular perturbation theory implies that normally hyperbolic portions of the so-called critical manifold, which is obtained for $\kappa = 0$ in (5), persist for κ positive and sufficiently small. However, since the geometry of that critical manifold degenerates in the limit as $\varepsilon \to 0$, a blow-up analysis in ε is performed to remove that degeneracy.

While our article is self-contained, we expect some familiarity on the part of the reader with geometric singular perturbation theory and the blow-up technique; see again [11,12,3,14] for details. For an introduction in the context of the present family of problems, the reader is referred to Appendix A of [13].

Remark 1. Since Equation (4c) can be written as $\frac{1}{\Gamma}U_\tau = (W - U)$, and since $\frac{\partial}{\partial U}(W - U) = -1$, the above quasi-steady-state assumption can be interpreted geometrically [4] as a global reduction to the critical manifold $\{W = U\}$, with singular perturbation parameter Γ^{-1}. For the value of Γ given in Table 1, that reduction is not justified, strictly speaking; however, we follow the biologically motivated reasoning in [9] here.

Our analysis of Equation (5) has some similarities to the study of the Goldbeter-Lefever model [21] in [13]; there, the critical manifold was found to consist of two non-hyperbolic lines and one normally hyperbolic line. The blow-up technique was then applied to achieve a complete desingularisation of the flow near that manifold, whereby the non-hyperbolic lines were blown up to intersecting cylinders, allowing the authors to prove the occurrence of relaxation oscillation in the system.

While Equation (5) shares some characteristics of the Goldbeter-Lefever model studied in [13], it is slightly more degenerate: as will turn out, the critical manifold here is the union of one non-hyperbolic line in the "inner" region and one normally hyperbolic curve in the "outer" region, which meet in a degenerate steady state at the origin. Moreover, the U-variable has to be scaled with the singular parameter ε due to the presence of the term $(U+\varepsilon)^2 + \Lambda R^2U^2$ in (5b), as ε cannot be eliminated by a simple change of coordinates, which represents the major conceptual difference to the model considered in [13]. Therefore, the resulting singularly perturbed structure is novel; our resolution of that structure, and in particular of the highly degenerate flow near the origin in (R, U, ε)-space, results in improved understanding of the

Table 1
Definition and numerical values, with orders of magnitude, of the parameters in (59); cf. [15], where the quantities in the second column are defined.

Parameter	Definition	Order of magnitude	Numerical value
κ	$\frac{k_2(1+L_2)}{k_i+k_t}$	$\ll 1$	0.0023
μ	$\frac{m_i+d}{m+1}$	$\ll 1 \sim d$	0.1274
ε	M^{-1}	$\ll 1$	0.1258
d	$\frac{1+L_1}{c+L_1}$	$\ll 1$	0.1
b	$\frac{\alpha q \sigma k_t}{(k_i+k_t)h}\frac{\lambda\theta}{1+\alpha\theta}$	$\ll 1$	0.01587
Γ	$\frac{k_e}{k_i+k_t}$	$\simeq 1$	2.1052
Λ	$(A\mu^2)^{-1}$	$\simeq 1$	0.2966
Θ	$\Lambda B\varepsilon$	$\simeq 1$ or $\gg 1$	1.5087
c		$\gg 1$	100
$\mathcal{P}$	$\frac{k_1}{k_2}$	$\gg 1$	100

oscillatory dynamics that is observed in the reformulated singular perturbation problem of cAMP signalling, Equation (5).

In accordance with the numerical values given in Table 1, we rescale the parameters $\mu = \tilde{\mu}\varepsilon^{\frac{1}{2}}$, $d = \tilde{d}\varepsilon^{\frac{1}{2}}$, and $b = \tilde{b}\varepsilon$ in (5). These scalings broadly agree with assumptions made in [15], where it was postulated that $\mu \sim d$, $\mu \simeq \varepsilon$, and $b \ll 1$; however, we rescale μ and d with $\varepsilon^{\frac{1}{2}}$ instead of with ε here, which is consistent with the basic geometry of oscillation found in [16] for the three-dimensional system, Equation (1). Moreover, we rewrite the resulting equations in the equivalent form

$$R' = \kappa(U+\mathcal{P}\varepsilon)\frac{(U+\varepsilon)^2+\Lambda R^2U^2}{(U+\varepsilon)(U+\frac{\varepsilon}{c})}\big[\tilde{\mu}\varepsilon^{\frac{1}{2}}(U+\varepsilon)-\big(U+\tilde{d}\varepsilon^{\frac{3}{2}}\big)R\big], \tag{6a}$$

$$U' = \tilde{b}\varepsilon^2(U+\varepsilon)^2+\Theta R^2U^2-U\big[(U+\varepsilon)^2+\Lambda R^2U^2\big], \tag{6b}$$

which is obtained by formally multiplying the right-hand sides in (5) with a (polynomial) factor of $(U+\varepsilon)^2+\Lambda R^2U^2$. (Since that factor is non-negative, the corresponding transformation of time does not change the direction of the flow.) Here, the prime now denotes differentiation with respect to the new, rescaled time.

Remark 2. The apparent singularity of Equation (6) at $(U,\varepsilon) = (0,0)$ will be resolved by blow-up; in fact, the right-hand side in (6a) vanishes to at least second order in (U,ε), which implies $\mathcal{C}^2$-smoothness of the corresponding vector field in both U and ε.

The following is the main result of our analysis:

Theorem 1. *Let $\varepsilon \in (0,\varepsilon_0]$, with ε_0 positive and sufficiently small. Then, there exists $\kappa_0 = \kappa_0(\varepsilon_0)$ such that, for $\kappa \in (0,\kappa_0]$, Equation (6) admits a unique family of attracting periodic orbits $\Gamma_{\kappa\varepsilon}$ which tends to a singular cycle $\Gamma_{0\varepsilon}$ as $\kappa \to 0$ uniformly for $\varepsilon \in (0,\varepsilon_0]$, and to a singular cycle Γ_{00} as $(\kappa,\varepsilon) \to (0,0)$.*

Remark 3. We emphasise that $\Gamma_{0\varepsilon}$ and Γ_{00} are defined implicitly, i.e., via $\Gamma_{\kappa\varepsilon}$, in the statement of Theorem 1; an explicit definition will be provided through the following analysis.

A visualisation of the assertions made in Theorem 1 can be found in Fig. 1, where the nullclines of Equation (6) are sketched in addition to the singular cycles Γ_{00} and $\Gamma_{0\varepsilon}$, as well as a sample periodic orbit $\Gamma_{\kappa\varepsilon}$ which was obtained numerically. Here, the values of the relevant parameters are as specified in Table 1, with the exception of $\kappa(=0.00023)$, $\mu(=0.13)$, and $d(=0.071)$; the latter two are chosen such that

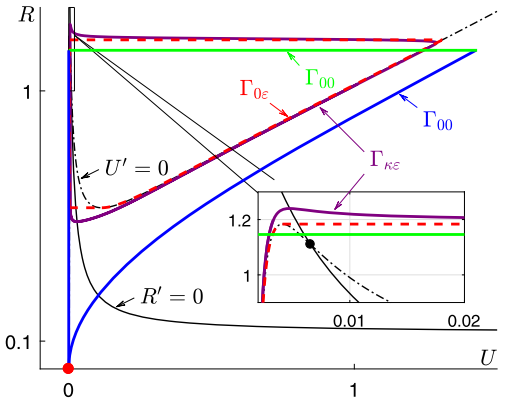

Fig. 1. Nullclines and periodic orbits for Equation (6), with parameter values as in Table 1: R-nullcline (solid black); U-nullcline (dash-dotted black); singular cycle Γ_{00} (solid blue; solid green); singular cycle $\Gamma_{0\varepsilon}$ (dashed red); periodic orbit $\Gamma_{\kappa\varepsilon}$ (solid purple); equilibrium (inset). (For interpretation of the colours in the figure(s), the reader is referred to the web version of this article.)

the unique equilibrium in the system is shifted to the middle branch of the U-nullcline, thus allowing for excitability and, hence, oscillatory dynamics.

In the remainder of the article, we will prove Theorem 1 by constructing a family of periodic (relaxation-type) cycles for Equation (6); as is common in singular perturbation theory, we will first identify a singular orbit when $\kappa = 0 = \varepsilon$. Subsequently, we will show the persistence of that orbit for κ and ε positive, but small. Our analysis follows that of Kosiuk and Szmolyan [13] in spirit, subject to the appropriate modifications due to differences in the singular structure of (6); in particular, our focus is on the resulting asymptotics in ε, which is discussed in detail, whereas the relatively standard perturbation analysis with respect to κ is treated in a more cursory fashion.

2. Singular dynamics

As Equation (6) for $\varepsilon > 0$ represents a slow-fast system in standard form, with singular perturbation parameter κ, we rewrite the corresponding flow on the slow time-scale to obtain the equivalent formulation

$$\dot{R} = (U + \mathcal{P}\varepsilon)\frac{(U+\varepsilon)^2 + \Lambda R^2 U^2}{(U+\varepsilon)(U+\frac{\varepsilon}{c})}\big[\tilde{\mu}\varepsilon^{\frac{1}{2}}(U+\varepsilon) - \big(U + \tilde{d}\varepsilon^{\frac{3}{2}}\big)R\big], \tag{7a}$$

$$\kappa\dot{U} = \tilde{b}\varepsilon^2(U+\varepsilon)^2 + \Theta R^2 U^2 - U\big[(U+\varepsilon)^2 + \Lambda R^2 U^2\big]. \tag{7b}$$

In our analysis, we hence first consider the singular limit of $\kappa = 0$ in Equations (6) and (7). The small-ε dynamics in that limit will be studied separately in different scaling regimes $\mathcal{R}_j$ $(j = 1, 2, 3)$, which are defined in Section 3 below.

2.1. Slow-fast analysis for $\kappa = 0$ and $\varepsilon > 0$

Setting $\kappa = 0$ in Equations (6) and (7) for fixed, positive ε defines two limiting systems, the "layer problem"

$$R' = 0, \tag{8a}$$

$$U' = \tilde{b}\varepsilon^2(U+\varepsilon)^2 + \Theta R^2 U^2 - U\big[(U+\varepsilon)^2 + \Lambda R^2 U^2\big] \tag{8b}$$

and the "reduced problem"

$$\dot{R} = (U+\mathcal{P}\varepsilon)\frac{(U+\varepsilon)^2+\Lambda R^2U^2}{(U+\varepsilon)(U+\frac{\varepsilon}{c})}\big[\tilde{\mu}\varepsilon^{\frac{1}{2}}(U+\varepsilon)-\big(U+\tilde{d}\varepsilon^{\frac{3}{2}}\big)R\big], \tag{9a}$$

$$0 = \tilde{b}\varepsilon^2(U+\varepsilon)^2+\Theta R^2U^2-U\big[(U+\varepsilon)^2+\Lambda R^2U^2\big]. \tag{9b}$$

The critical manifold $\mathcal{S}_{0\varepsilon}$, which is defined by (9b), is precisely the U-nullcline in Equation (6). The manifold $\mathcal{S}_{0\varepsilon}$ is S-shaped; linearisation of the layer problem, Equation (8), about $\mathcal{S}_{0\varepsilon}$ shows that $\frac{\partial}{\partial U}\big\{\tilde{b}\varepsilon^2(U+\varepsilon)^2+\Theta R^2U^2-U\big[(U+\varepsilon)^2+\Lambda R^2U^2\big]\big\}$ has zeroes at $U^A_{0\varepsilon}=2\tilde{b}\varepsilon^2+\mathcal{O}(\varepsilon^3)$ and $U^C_{0\varepsilon}=\varepsilon+\mathcal{O}(\varepsilon^2)$. Hence, $\mathcal{S}_{0\varepsilon}$ consists of three branches, which are separated by two fold points at $A_{0\varepsilon}:\big(R^A_{0\varepsilon},U^A_{0\varepsilon}\big)$ and $C_{0\varepsilon}:\big(R^C_{0\varepsilon},U^C_{0\varepsilon}\big)$, with $R^A_{0\varepsilon}=\frac{1}{2\sqrt{\Theta b}}+\mathcal{O}(\varepsilon)$ and $R^C_{0\varepsilon}=\frac{2}{\sqrt{\Theta}}\varepsilon^{\frac{1}{2}}+\mathcal{O}(\varepsilon)$; the left branch $\mathcal{S}^{a-}_{0\varepsilon}$ and the right branch $\mathcal{S}^{a+}_{0\varepsilon}$ are attracting under the layer flow of Equation (6), while the middle branch $\mathcal{S}^{r}_{0\varepsilon}$ is repelling.

Remark 4. For ε non-small in the statement of Theorem 1, Equation (6) admits standard relaxation-type cycles [17] for $\kappa\in(0,\kappa_0]$ sufficiently small, with $\kappa_0=\kappa_0(\varepsilon)$, as long as the critical manifold $\mathcal{S}_{0\varepsilon}$ remains S-shaped; in fact, for the parameter values given in Table 1, that is the case for ε up to the order of 10. However, our focus here is on ε small, due to the degenerate singular structure of $\mathcal{S}_{0\varepsilon}$ as $\varepsilon\to 0$; see Section 2.2 below.

We denote the unique equilibrium of (6), which is found in the intersection of the R-nullcline with $\mathcal{S}_{0\varepsilon}$, by $E_{0\varepsilon}$; see Fig. 2. (Due to our assumptions on the parameters μ, d, and Θ, $E_{0\varepsilon}$ is, in fact, located on the middle branch $\mathcal{S}^r_{0\varepsilon}$ of $\mathcal{S}_{0\varepsilon}$.) Analysis of the reduced flow on $\mathcal{S}_{0\varepsilon}$ shows that R increases below the point $A_{0\varepsilon}$ on $\mathcal{S}^{a-}_{0\varepsilon}$, while it decreases on $\mathcal{S}^{a+}_{0\varepsilon}$. (The direction of the flow on $\mathcal{S}^r_{0\varepsilon}$, as indicated in Fig. 2, is determined by the sign of the term $\big[\tilde{\mu}\varepsilon^{\frac{1}{2}}(U+\varepsilon)-\big(U+\tilde{d}\varepsilon^{\frac{3}{2}}\big)R\big]$ in (9a).) Hence, we obtain the following standard singular relaxation-type dynamics for $\kappa=0$ and fixed, positive ε: orbits starting on $\mathcal{S}^{a-}_{0\varepsilon}$ jump at the fold point $A_{0\varepsilon}$ and reach a point $D_{0\varepsilon}$ on $\mathcal{S}^{a+}_{0\varepsilon}$ along the 1-dimensional stable manifold thereof; they then follow the reduced dynamics on $\mathcal{S}^{a+}_{0\varepsilon}$ until they reach the fold point at $C_{0\varepsilon}$, from where they jump back to a point $B_{0\varepsilon}$ on $\mathcal{S}^{a-}_{0\varepsilon}$ along the 1-dimensional stable manifold thereof; finally, they follow the reduced dynamics on $\mathcal{S}^{a-}_{0\varepsilon}$ until they reach $A_{0\varepsilon}$, at which point the above oscillation repeats. Correspondingly, we define the singular cycle $\Gamma_{0\varepsilon}$, which consists of the heteroclinic orbit $\Gamma^{AD}_{0\varepsilon}$ connecting $A_{0\varepsilon}$ to $D_{0\varepsilon}$ under the layer flow of (8), the segment $\Gamma^{DC}_{0\varepsilon}$ of $\mathcal{S}^{a+}_{0\varepsilon}$ from $D_{0\varepsilon}$ to $C_{0\varepsilon}$, the heteroclinic orbit $\Gamma^{CB}_{0\varepsilon}$ connecting $C_{0\varepsilon}$ to $B_{0\varepsilon}$ under the layer flow, and the segment $\Gamma^{BA}_{0\varepsilon}$ of $\mathcal{S}^{a-}_{0\varepsilon}$ between $B_{0\varepsilon}$ and $A_{0\varepsilon}$; cf. again Fig. 2.

Remark 5. Here and in the following, reduced dynamics is depicted in blue, while the corresponding layer flow is shown in green; double arrows indicate hyperbolicity, while non-hyperbolic dynamics is indicated with single arrows.

It follows from [14, Theorem 2.3] that $\Gamma_{0\varepsilon}$ persists, for ε positive and fixed and κ sufficiently small, as an attracting relaxation-type cycle of Equation (6). However, as (6) constitutes a two-parameter singular perturbation problem, we are interested in the double limit as κ and ε tend to zero simultaneously.

2.2. Slow-fast analysis for $\kappa=0=\varepsilon$

As will turn out, the limit as $(\kappa,\varepsilon)\to(0,0)$ in Equation (6) is significantly more singular than the limit of $\kappa\to 0$ with ε fixed, as considered in the previous subsection.

For $(\kappa,\varepsilon)=(0,0)$, (6) yields the seemingly simple layer problem

$$R' = 0, \tag{10a}$$

$$U' = \Theta R^2U^2-U(U^2+\Lambda R^2U^2), \tag{10b}$$

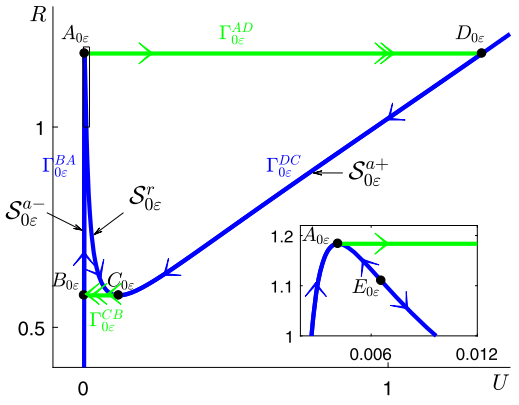

Fig. 2. Reduced flow on the critical manifold $\mathcal{S}_{0\varepsilon}$ (solid blue), layer dynamics (solid green), singular cycle $\Gamma_{0\varepsilon}$ (solid blue; solid green), and equilibrium $E_{0\varepsilon}$ (inset) for Equation (8), with parameter values as in Table 1.

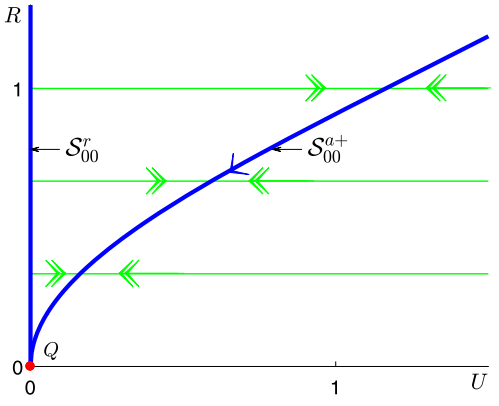

Fig. 3. Reduced flow on the critical manifold $\mathcal{S}_{00}$ (solid blue), layer dynamics (solid green), and non-hyperbolic origin Q (red dot) for Equation (10).

which corresponds precisely to the system that is obtained from (8) for $\varepsilon = 0$. Equation (10) admits two sets of equilibria; one of these satisfies $U = 0$, while the other is defined by $\Theta R^2 - (U + \Lambda R^2 U) = 0$. Hence, the critical manifold $\mathcal{S}_{00}$ for (10) consists of the curves $\mathcal{S}^r_{00} = \{(R,0) \,|\, R > 0\}$ and $\mathcal{S}^{a+}_{00} = \{(R,U) \,|\, R > 0,\ U = \frac{\Theta R^2}{1+\Lambda R^2}\}$, which meet in the origin Q. (Clearly, $\mathcal{S}_{00}$ coincides with the critical manifold $\mathcal{S}_{0\varepsilon}$ when $\varepsilon = 0$.) Linearisation of Equation (10) about $\mathcal{S}_{00}$ shows that the curve $\mathcal{S}^{a+}_{00}$ is normally hyperbolic, while $\mathcal{S}^r_{00}$ – the R-axis – and the point Q are non-hyperbolic; see Fig. 3 for an illustration.

In particular, it follows that, for U and R bounded away from zero, the critical manifold $\mathcal{S}^{a+}_{0\varepsilon}$ introduced in the previous subsection is a regular perturbation (in ε) of the manifold $\mathcal{S}^{a+}_{00}$ defined above. Hence, standard theory [4] can be applied to show the persistence of $\mathcal{S}^{a+}_{00}$ for κ and ε positive and small in that case:

Proposition 1. *Let $\varepsilon \in [0, \varepsilon_0]$ be fixed, and let $\kappa \in [0, \kappa_0]$, with ε_0 and κ_0 positive and sufficiently small. Moreover, let $U \in [\underline{\alpha}, \bar{\alpha}]$ and $R \in [\underline{\beta}, \bar{\beta}]$, where $\underline{\alpha}$ and $\underline{\beta}$ are positive and small, but independent of (κ, ε), and $\bar{\alpha}$ and $\bar{\beta}$ are assumed to be $\mathcal{O}(1)$. Then, the following statements hold:*

1. *For $\kappa = 0$, Equation (8) admits the critical manifold*

$$\mathcal{S}^{a+}_{0\varepsilon} = \{(R,U) \,|\, R \in [\underline{\beta}, \bar{\beta}],\ U = \Phi_{0\varepsilon}(R)\}; \tag{11}$$

here, the function $\Phi_{0\varepsilon}$ satisfies

$$\Phi_{0\varepsilon}(R) = \frac{\Theta R^2}{1+\Lambda R^2} + \frac{\tilde{b}}{1+\Lambda R^2}\varepsilon^2 + \mathcal{O}(\varepsilon^3).$$

2. *The manifold* $\mathcal{S}^{a+}_{0\varepsilon}$ *is normally attracting, with a single negative eigenvalue* $-\frac{\Theta^2 R^4}{1+\Lambda R^2}$.
3. *The reduced flow on* $\mathcal{S}^{a+}_{0\varepsilon}$ *is given by*

$$\dot{R} = -\frac{\Theta^2 R^5}{1+\Lambda R^2} + \frac{\Theta^2 R^4 \tilde{\mu}}{1+\Lambda R^2}\sqrt{\varepsilon} + \mathcal{O}(\varepsilon),$$

which implies, in particular, $\dot{R} < 0$ *for* ε *sufficiently small.*
4. *For* κ *positive and small, the manifold* $\mathcal{S}^{a+}_{0\varepsilon}$ *perturbs to a manifold*

$$\mathcal{S}^{a+}_{\kappa\varepsilon} = \big\{(R,U)\,\big|\, R \in [\underline{\beta}, \bar{\beta}],\ U = \Phi_{\kappa\varepsilon}(R)\big\}, \tag{12}$$

where $\Phi_{\kappa\varepsilon} = \Phi_{0\varepsilon} + \mathcal{O}(\kappa)$ *is regular in* (κ,ε) *to any order therein.*

Remark 6. Comparison of Figs. 2 and 3 shows that the manifolds $\mathcal{S}^{a-}_{0\varepsilon}$ and $\mathcal{S}^{r}_{0\varepsilon}$ merge into $\mathcal{S}^{r}_{00}$ in the limit as $\varepsilon \to 0$; correspondingly, the points $B_{0\varepsilon}$ and $C_{0\varepsilon}$ coalesce into the origin Q in that limit.

3. Scaling regimes

The discussion in Section 2 indicates that, for $\varepsilon = 0$, essential portions of the sought-after relaxation cycle $\Gamma_{\kappa\varepsilon}$ for Equation (6) are "hidden" in the non-hyperbolic line $\mathcal{S}^{r}_{00}$ and the point Q; specifically, it is intuitively clear that $\mathcal{S}^{a-}_{0\varepsilon}$ and $\mathcal{S}^{r}_{0\varepsilon}$ merge into $\mathcal{S}^{r}_{00}$ in that limit, while the fold point $C_{0\varepsilon}$ converges to the origin Q. Appropriate rescalings of R and U are required in order to make these aspects of the dynamics visible in different scaling regimes. These regimes are denoted by $\mathcal{R}_j$ $(j = 1,2,3)$, and are defined as follows:

(1) Regime $\mathcal{R}_1$: $U = \mathcal{O}(\varepsilon^2)$, $R = \mathcal{O}(1)$;
(2) Regime $\mathcal{R}_2$: $U = \mathcal{O}(\varepsilon)$, $R = \mathcal{O}(\varepsilon^{\frac{1}{2}})$;
(3) Regime $\mathcal{R}_3$: $U = \mathcal{O}(1)$, $R = \mathcal{O}(1)$.

In particular, the "inner" and "outer" regions, which are mentioned in the Introduction, are covered by regimes $\mathcal{R}_j$ $(j = 1,2)$ and regime $\mathcal{R}_3$, respectively; see Fig. 4. The above scalings in U then also imply the corresponding scalings of R, and can be substantiated via the method of Newton polygons [2], which shows in particular that the parameter b must be of the order $\mathcal{O}(\varepsilon)$, as assumed above. Finally, the scalings in regimes $\mathcal{R}_1$ and $\mathcal{R}_2$ are consistent with the ε-dependence of the two fold points of Equation (6) at $A_{0\varepsilon}$ and $C_{0\varepsilon}$, respectively – or, rather, of the (R,U)-coordinates thereof.

In this section, we will discuss the geometry in the three regimes $\mathcal{R}_j$ $(j = 1,2,3)$ in turn to motivate how the "full" singular dynamics of Equation (6) can be desingularised to allow for a description of the resulting, global oscillation. Our discussion will be made fully rigorous in subsequent sections, where a desingularisation will be achieved via the blow-up technique. In particular, as the three regimes introduced above do not overlap, it is not *a priori* evident how to match them; here, we will show that matching can be accomplished in various coordinate charts – so-called "phase-directional charts" – after blow-up, as was also done in [13]. (We emphasise that these charts are not covered by the scaling regimes themselves, which correspond to "rescaling charts" in the blow-up, but that they arise naturally in our blow-up analysis.)

3.1. Regime $\mathcal{R}_1$: $U = \mathcal{O}(\varepsilon^2)$, $R = \mathcal{O}(1)$

Regime $\mathcal{R}_1$ covers a neighbourhood of the R-axis that is, however, bounded away from the origin Q. Correspondingly, we introduce the scaling

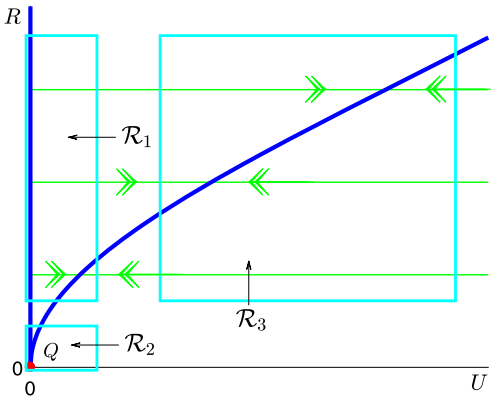

Fig. 4. The scaling regimes $\mathcal{R}_1$, $\mathcal{R}_2$, and $\mathcal{R}_3$ for Equation (6).

$$R = R_1 \quad \text{and} \quad U = \varepsilon^2 U_1 \tag{13}$$

in that regime. For the sake of definiteness, we assume that $U_1 \in [0, \bar{\alpha}_1]$ and $R_1 \in [\underline{\beta}_1, \bar{\beta}_1]$, where $\bar{\alpha}_1$ is assumed to be large, $\underline{\beta}_1$ is small, and $\bar{\beta}_1$ is $\mathcal{O}(1)$, corresponding to our assumption that the original variables U and R satisfy $U = \mathcal{O}(\varepsilon^2)$ and $R = \mathcal{O}(1)$; see Fig. 5.

After dividing out the factor ε^2, we obtain the following system of equations from Equation (6):

$$R_1' = \kappa\varepsilon^{\frac{1}{2}}(\varepsilon U_1 + \mathcal{P})\frac{(\varepsilon U_1+1)^2 + \Lambda R_1^2\varepsilon^2 U_1^2}{(\varepsilon U_1+1)(\varepsilon U_1 + \frac{1}{c})}\big[\tilde{\mu}(\varepsilon U_1+1) - \big(\varepsilon^{\frac{1}{2}}U_1 + \tilde{d}\big)R_1\big], \tag{14a}$$

$$U_1' = \tilde{b}(\varepsilon U_1+1)^2 + \Theta R_1^2 U_1^2 - U_1\big[(\varepsilon U_1+1)^2 + \Lambda R_1^2\varepsilon^2 U_1^2\big], \tag{14b}$$

which represents a slow-fast system in standard form for κ small.

When $\kappa = 0$, Equation (14) yields the layer problem

$$R_1' = 0, \tag{15a}$$

$$U_1' = \tilde{b}(\varepsilon U_1+1)^2 + \Theta R_1^2 U_1^2 - U_1\big[(\varepsilon U_1+1)^2 + \Lambda R_1^2\varepsilon^2 U_1^2\big]; \tag{15b}$$

considering the limit of $\varepsilon = 0$ in (15), we obtain

$$R_1' = 0, \tag{16a}$$

$$U_1' = \tilde{b} + \Theta R_1^2 U_1^2 - U_1. \tag{16b}$$

The critical manifold for Equation (16) is defined by $\tilde{b} + \Theta R_1^2 U_1^2 - U_1 = 0$; we denote that manifold as $\mathcal{S}_{00_1}$. The manifold $\mathcal{S}_{00_1}$ consists of a left attracting branch $\mathcal{S}_{00_1}^{a-}$, where $U_1 < 2\tilde{b}$, and a right repelling branch $\mathcal{S}_{00_1}^{r}$ with $U_1 > 2\tilde{b}$; these two branches are separated by a fold point at $A_{00_1} : \left(\frac{1}{2\sqrt{\Theta\tilde{b}}}, 2\tilde{b}\right)$. The branch $\mathcal{S}_{00_1}^{r}$ is asymptotic to the U_1-axis as $U_1 \to \infty$, while the branch $\mathcal{S}_{00_1}^{a-}$ intersects the U_1-axis in the point $B_{00_1} : (0, \tilde{b})$. Orbits starting close to the U_1-axis are rapidly attracted to $\mathcal{S}_{00_1}^{a-}$; they then follow the reduced dynamics until they reach the fold point A_{00_1}, where they jump in the positive U_1-direction along an orbit of the layer problem, Equation (15). The geometry in regime $\mathcal{R}_1$ is summarised in Fig. 5; for details on the passage past a singularly perturbed planar fold, the reader is referred to [14], as well as to the summary in Appendix A of [13]. In particular, standard theory [4] implies that $\mathcal{S}_{00_1}^{a-}$ and $\mathcal{S}_{00_1}^{r}$ will persist as slow manifolds away from A_{00_1}, for κ positive and small.

Remark 7. We note that the steady state E_{0_ε} is not visible in regime $\mathcal{R}_1$: given our choice of μ and d, with $\frac{\tilde{\mu}}{\tilde{d}} > \frac{1}{2\sqrt{\Theta\tilde{b}}}$, the equation $\{\tilde{b} + \Theta R_1^2 U_1^2 - U_1 = 0\}\big|_{\{R_1 = \frac{\tilde{\mu}}{\tilde{d}}\}}$ admits no real solutions for U_1; the underlying reason

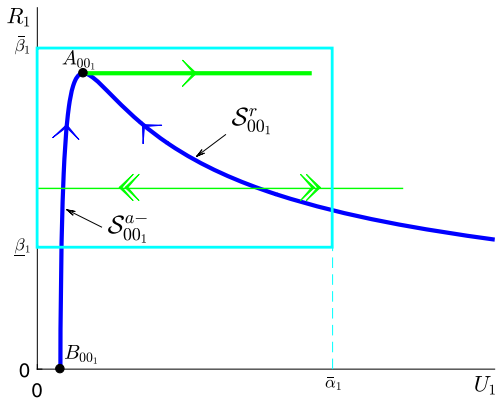

Fig. 5. Reduced flow on the critical manifold $\mathcal{S}_{00_1}$ (solid blue) and layer dynamics (solid green) in regime $\mathcal{R}_1$.

is the scaling of the U-coordinate of E_{0_ε}, which is identified in regime $\mathcal{R}_2$ in the subsequent subsection. In particular, it follows that the reduced flow in the R_1-variable is directed upwards to A_{00_1} on $\mathcal{S}_{00_1}$.

Remark 8. The critical manifold $\mathcal{S}_{00_1}$ corresponds to appropriately specified portions of $\mathcal{S}^{a-}_{0\varepsilon}$ and $\mathcal{S}^r_{0\varepsilon}$, as defined in Section 2.1, in the limit as $\varepsilon \to 0$, while the fold point A_{00_1} corresponds to $A_{0\varepsilon}$ in that limit. (Here, we note that $\mathcal{S}_{00_1}$ perturbs in a regular fashion for ε positive and small.) In some sense, to be specified later, the point $C_{0\varepsilon}$ is retrieved for $U_1 \to \infty$ on $\mathcal{S}^r_{0\varepsilon_1}$ in the limit of $\varepsilon = 0$.

3.2. Regime $\mathcal{R}_2$: $U = \mathcal{O}(\varepsilon)$, $R = \mathcal{O}(\varepsilon^{\frac{1}{2}})$

Regime $\mathcal{R}_2$ covers a neighbourhood of the origin Q; recall Fig. 4. We introduce the scaling

$$R = \varepsilon^{\frac{1}{2}} R_2 \quad \text{and} \quad U = \varepsilon U_2; \tag{17}$$

here, we assume that $U_2 \in [0, \bar{\alpha}_2]$ and $R_2 \in [0, \bar{\beta}_2]$, where $\bar{\alpha}_2$ and $\bar{\beta}_2$ are large, corresponding to our assumption that the original variables U and R satisfy $U = \mathcal{O}(\varepsilon)$ and $R = \mathcal{O}(\varepsilon^{\frac{1}{2}})$, respectively.

After division through a factor of ε^2, Equation (6) becomes

$$R_2' = \kappa(U_2 + \mathcal{P}) \frac{(U_2+1)^2 + \Lambda\varepsilon R_2^2 U_2^2}{(U_2+1)(U_2+\frac{1}{c})} \big[\tilde{\mu}(U_2+1) - \big(U_2 + \tilde{d}\varepsilon^{\frac{1}{2}}\big) R_2\big], \tag{18a}$$

$$U_2' = \tilde{b}\varepsilon(U_2+1)^2 + \Theta R_2^2 U_2^2 - U_2\big[(U_2+1)^2 + \Lambda\varepsilon R_2^2 U_2^2\big], \tag{18b}$$

which again represents a slow-fast system for κ small.

The layer problem obtained for $\kappa = 0$ now reads

$$R_2' = 0, \tag{19a}$$

$$U_2' = \tilde{b}\varepsilon(U_2+1)^2 + \Theta R_2^2 U_2^2 - U_2\big[(U_2+1)^2 + \Lambda\varepsilon R_2^2 U_2^2\big]; \tag{19b}$$

setting $\varepsilon = 0$ in (19), we find the simplified system

$$R_2' = 0, \tag{20a}$$

$$U_2' = \Theta R_2^2 U_2^2 - U_2(U_2+1)^2. \tag{20b}$$

The corresponding critical manifold, which is denoted as $\mathcal{S}_{00_2}$, is defined by $\Theta R_2^2 U_2^2 - U_2(U_2+1)^2 = 0$. The manifold $\mathcal{S}_{00_2}$ consists of a left attracting branch $\mathcal{S}^{a-}_{00_2}$, corresponding to $\{U_2 = 0\}$, a middle repelling

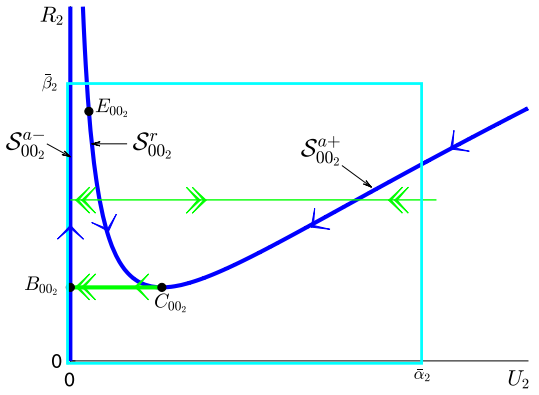

Fig. 6. Reduced flow on the critical manifold $\mathcal{S}_{00_2}$ (solid blue), layer dynamics (solid green), and equilibrium E_{00_2} in regime $\mathcal{R}_2$.

branch $\mathcal{S}^r_{00_2}$, with $0 < U_2 < 1$, and a right attracting branch $\mathcal{S}^{a+}_{00_2}$, where $U_2 > 1$. The branches $\mathcal{S}^r_{00_2}$ and $\mathcal{S}^{a+}_{00_2}$ are separated by a fold point at C_{00_2} : $\left(\frac{2}{\sqrt{\Theta}}, 1\right)$. Orbits follow the slow flow on the branch $\mathcal{S}^{a+}_{00_2}$ until they reach C_{00_2}, where they jump to a point B_{00_2} on $\mathcal{S}^{a-}_{00_2}$ and then follow the slow flow on $\mathcal{S}^{a-}_{00_2}$; see Fig. 6 for an illustration. We note that the fold point $A_{0\varepsilon}$ – and, hence, the fast jump to $D_{0\varepsilon}$ – is not visible in this regime. Finally, by our assumptions on the parameters μ and Θ, the steady state at E_{00_2} : $\left(\Theta\tilde{\mu}^2, \tilde{\mu} + \frac{1}{\Theta\tilde{\mu}}\right)$ is located on the middle repelling branch $\mathcal{S}^r_{00_2}$. (That state is found in the intersection of $\mathcal{S}_{00_2}$ with the R_2-nullcline $\left\{R_2 = \frac{\tilde{\mu}(U_2+1)}{U_2}\right\}$.) Again, geometric singular perturbation theory [4] implies the persistence of $\mathcal{S}^{a-}_{00_2}$, $\mathcal{S}^r_{00_2}$, and $\mathcal{S}^{a+}_{00_2}$ for κ positive and small, uniformly in ε, away from the fold point C_{00_2}, while standard results on passage past a singularly perturbed planar fold [14] apply at C_{00_2}.

Remark 9. Fig. 2 seems to be in contradiction with Figs. 5 and 6, as it indicates that $E_{0\varepsilon}$ is located near the fold point $A_{0\varepsilon}$, rather than close to $C_{0\varepsilon}$. However, that seeming discrepancy is due to the fixed, relatively large, value of $\varepsilon = 0.12$ in Fig. 2, recall Table 1, whereas Figs. 5 and 6 illustrate the singular limit of $\varepsilon = 0$.

Remark 10. The critical manifold $\mathcal{S}_{00_2}$ corresponds to appropriately specified portions of $\mathcal{S}^{a-}_{0\varepsilon}$, $\mathcal{S}^r_{0\varepsilon}$, and $\mathcal{S}^{a+}_{0\varepsilon}$, as defined in Section 2.1, in the limit as $\varepsilon \to 0$. In particular, the fold point C_{00_2} corresponds to $C_{0\varepsilon}$ in that limit, while the point B_{00_2} is equivalent to $B_{0\varepsilon}$. The jump point at $D_{0\varepsilon}$ corresponds to the limit as $U_2 \to \infty$ on $\mathcal{S}^{a+}_{00_2}$, while the fold point $A_{0\varepsilon}$ is found in the limit as $R_2 \to \infty$ on $\mathcal{S}^{a-}_{00_2}$.

3.3. Regime $\mathcal{R}_3$: $U = \mathcal{O}(1)$, $R = \mathcal{O}(1)$

In regime $\mathcal{R}_3$, Equation (6) depends on ε in a regular fashion. We consider $U_3 \in [\underline{\alpha}_3, \bar{\alpha}_3]$ and $R_3 \in [\underline{\beta}_3, \bar{\beta}_3]$ here, where $\underline{\alpha}_3$ and $\underline{\beta}_3$ are positive and small and $\bar{\alpha}_3$ and $\bar{\beta}_3$ are assumed to be $\mathcal{O}(1)$, corresponding to our assumption that the original variables U and R are $\mathcal{O}(1)$ in the "outer" region. For $\kappa = 0$ in (6), we obtain the layer problem given in (15), while the limit of $\varepsilon = 0$ yields the singular layer problem

$$R_3' = 0, \tag{21a}$$

$$U_3' = \Theta R_3^2 U_3^2 - U_3^3(1 + \Lambda R_3^2). \tag{21b}$$

The critical manifold for Equation (21), which we denote as $\mathcal{S}^{a+}_{00_3}$, is defined by $\Theta R_3^2 - U_3(1 + \Lambda R_3^2) = 0$, and is normally attracting. Since the reduced flow on $\mathcal{S}^{a+}_{00_3}$ for $\varepsilon = 0$ reads

$$\dot{R}_3 = -U_3^2 R_3(1 + \Lambda R_3^2), \tag{22}$$

R_3 is decreasing on $\mathcal{S}^{a+}_{00_3}$; see Fig. 7.

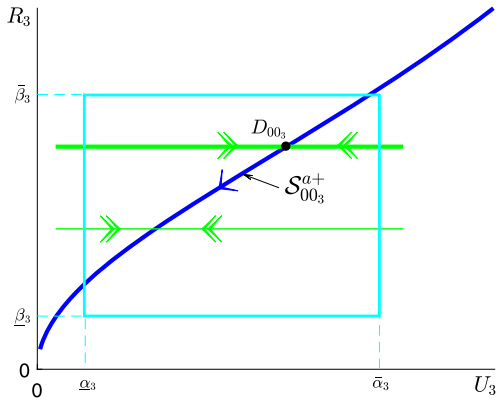

Fig. 7. Reduced flow on the critical manifold $\mathcal{S}^{a+}_{00_3}$ (solid blue) and layer dynamics (solid green) in regime $\mathcal{R}_3$.

For $\varepsilon > 0$, the curve $\mathcal{S}^{a+}_{00_3}$ perturbs in a regular fashion to the analogue, in regime $\mathcal{R}_3$, of the family of saddle-type critical manifolds that was denoted by $\mathcal{S}^{a+}_{0\varepsilon}$ in Section 2.1. Standard theory [4] implies that orbits to the left of the critical manifold $\mathcal{S}^{a+}_{00_3}$ are rapidly attracted by the slow manifold corresponding to $\mathcal{S}^{a+}_{00_3}$; they then follow the slow flow on that manifold.

Remark 11. In the limit as $\varepsilon \to 0$, the critical manifold $\mathcal{S}^{a+}_{00_3}$ corresponds to the portion of $\mathcal{S}^{a+}_{0\varepsilon}$ where U_3 and R_3 are $\mathcal{O}(1)$. The point D_{00_3} corresponds to the point $D_{0\varepsilon}$ in that limit, while the singular orbit connecting the point A_{00_3} – which is not visible in this regime – to D_{00_3} corresponds to the saddle-type fibre of the point D_{0_ε} in the limit as $\varepsilon \to 0$.

3.4. Summary

Combining our discussion of the three regimes $\mathcal{R}_j$ $(j = 1, 2, 3)$, we define the singular cycle Γ_{00} for Equation (6) in the limit of $(\kappa, \varepsilon) = (0, 0)$ as

$$\Gamma_{00} = \Gamma^{AD}_{00} \cup \Gamma^{DQ}_{00} \cup \Gamma^{QA}_{00},$$

where the orbit Γ^{AD}_{00} corresponds to the fast fibre of (8) that connects the points $A_{00} : \left(\frac{1}{2\sqrt{\Theta\bar{b}}}, 0\right)$ and $D_{00} : \left(\frac{1}{2\sqrt{\Theta\bar{b}}}, \frac{\Theta}{4\Theta\bar{b}+\Lambda}\right)$, the orbit Γ^{DQ}_{00} denotes the segment of the critical manifold $\mathcal{S}^{a+}_{00}$ between the points D_{00} and $Q_{00} : (0, 0)$, and Γ^{QA}_{00} is the segment of the critical manifold $\mathcal{S}^{r}_{00}$ between the points Q_{00} and A_{00}; see Fig. 8. We emphasise again that no reduced flow can be meaningfully defined on $\mathcal{S}^{r}_{00}$, i.e., that the segment Γ^{QA}_{00} is degenerate; that degeneracy will be partially resolved by blow-up.

For $(\kappa, \varepsilon) \to (0, 0)$, regime $\mathcal{R}_1$ collapses onto the non-hyperbolic line $\mathcal{S}^{r}_{00}$, while regime $\mathcal{R}_2$ shrinks to the non-hyperbolic origin; in particular, the points B_{00} and C_{00} coalesce into Q_{00} in the double singular limit, as the fast fibre connecting them vanishes. In regime $\mathcal{R}_3$, on the other hand, that limit is regular, as can be seen from the fact that the manifold $\mathcal{S}^{a+}_{00}$ remains normally attracting.

In conclusion, the degenerate geometry of Γ_{00} has hence been locally resolved in the scaling regimes $\mathcal{R}_j$ $(j = 1, 2, 3)$; however, to obtain a global picture, we investigate the transition between these regimes via a combination of geometric singular perturbation theory and the blow-up technique. Our geometric approach seems ideally suited to such an investigation, as it yields a uniformly valid and intuitively appealing description of relaxation-type oscillation in the two-parameter singular perturbation problem, Equation (6).

Remark 12. We note that the curves of equilibria Γ^{QA}_{00} and Γ^{DQ}_{00} for (10) can be connected by the corresponding layer flow for any fixed choice of R, allowing for a continuum of singular cycles. However, the analysis

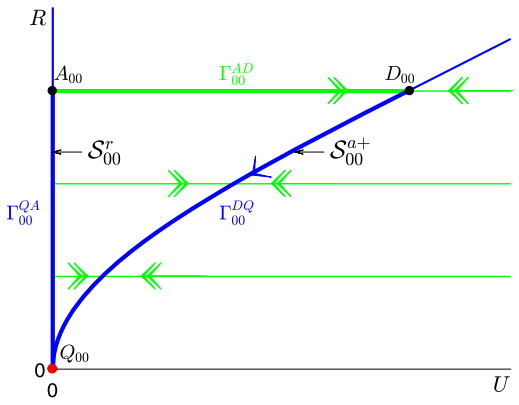

Fig. 8. Reduced flow on the critical manifold $\mathcal{S}_{00}$ (solid blue), layer dynamics (solid green), non-hyperbolic origin Q_{00} (red dot), and singular cycle Γ_{00} (solid blue; solid green) for Equation (10).

in regime $\mathcal{R}_1$ suggests that Γ_{00}, as defined above, is the appropriate choice, which will be substantiated by blow-up in the following section.

4. Blow-up analysis

Given the highly singular nature of Equation (6) in regimes $\mathcal{R}_1$ and $\mathcal{R}_2$, we apply the blow-up technique to desingularise the dynamics in a neighbourhood of the non-hyperbolic R-axis, with a particular focus on the degenerate equilibrium at the origin. To that end, we consider the augmented vector field that is obtained by appending the trivial equation $\varepsilon' = 0$ in (6):

$$R' = \kappa(U + \mathcal{P}\varepsilon)\frac{(U+\varepsilon)^2 + \Lambda R^2 U^2}{(U+\varepsilon)(U+\frac{\varepsilon}{c})}\big[\tilde{\mu}\varepsilon^{\frac{1}{2}}(U+\varepsilon) - \big(U + \tilde{d}\varepsilon^{\frac{3}{2}}\big)R\big], \tag{23a}$$

$$U' = \tilde{b}\varepsilon^2(U+\varepsilon)^2 + \Theta R^2 U^2 - U\big[(U+\varepsilon)^2 + \Lambda R^2 U^2\big], \tag{23b}$$

$$\varepsilon' = 0. \tag{23c}$$

As is conventional in the application of blow-up, the parameter ε is now treated as an additional state variable in the above augmented system, while κ encodes the separation of scales, as before. Our analysis will proceed in two steps: first, we will blow up the origin in the extended (R, U, ε)-space to a sphere, which will allow us to give a rigorous description of the dynamics in regime $\mathcal{R}_2$; the non-hyperbolic line $\mathcal{S}_{00}^r$ – which corresponds to regime $\mathcal{R}_1$ – will be recovered in one of the phase-directional charts in that blow up, and will be desingularised via a second (cylindrical) blow-up transformation. The dynamics that is obtained in the various coordinate charts after blow-up will then be combined into a global description of the flow of Equation (6) near the degenerate R-axis that is uniformly valid in both κ and ε.

Finally, we note that the phase space of (6) can be viewed as being foliated in $\varepsilon \in [0, \varepsilon_0]$, for ε_0 positive and small. Correspondingly, the family of critical manifolds $\mathcal{S}_{0\varepsilon} = \mathcal{S}_{0\varepsilon}^{a-} \cup \mathcal{S}_{0\varepsilon}^{r} \cup \mathcal{S}_{0\varepsilon}^{a+}$ defined in Section 2.1 can be viewed as a two-dimensional critical manifold $\mathcal{S}_0$, with folds along the curves $\mathcal{F}_0^A := \big\{(A_{0\varepsilon}, \varepsilon) \,\big|\, \varepsilon \in [0, \varepsilon_0]\big\}$ and $\mathcal{F}_0^C := \big\{(C_{0\varepsilon}, \varepsilon) \,\big|\, \varepsilon \in [0, \varepsilon_0]\big\}$.

4.1. Blow-up of the degenerate origin

We recall that regime $\mathcal{R}_2$ corresponds to the scaling $U = \mathcal{O}(\varepsilon)$ and $R = \mathcal{O}(\varepsilon^{\frac{1}{2}})$; cf. Section 3.2. In view of these scalings, we introduce the following quasi-homogeneous blow-up transformation of the origin in Equation (23):

$$R = \rho\bar{r}, \quad U = \rho^2\bar{u}, \quad \text{and} \quad \varepsilon = \rho^2\bar{\varepsilon}, \tag{24}$$

with $(\bar{r}, \bar{u}, \bar{\varepsilon}) \in \mathbb{S}^2$ and $\rho \in [0, \rho_0]$, for ρ_0 positive and small. In other words, the degenerate origin in (R, U, ε)-space corresponding to $\rho = 0$ in Equation (24) is blown up to the 2-sphere in $\mathbb{R}^3$. The vector field that is induced by Equation (23) after blow-up is conventionally studied in appropriate coordinate charts [3,14] that cover different parts of the blown-up space. We will require two charts in our analysis, which we denote by K_1 and K_2; these charts are obtained for $\bar{r} = 1$ and $\bar{\varepsilon} = 1$ in (24), respectively, which implies

$$R = \rho_1, \quad U = \rho_1^2 u_1, \quad \text{and} \quad \varepsilon = \rho_1^2\varepsilon_1 \tag{25}$$

and

$$R = \rho_2 r_2, \quad U = \rho_2^2 u_2, \quad \text{and} \quad \varepsilon = \rho_2^2, \tag{26}$$

respectively, for the coordinates in these charts. Intuitively speaking, chart K_1 hence covers a neighbourhood of parts of the equator of the blow-up sphere $\mathbb{S}^2 \times \{0\}$ where $R > 0$ holds, while the top of that sphere, with $\varepsilon > 0$, is described in chart K_2; see Fig. 12 below for an illustration.

Remark 13. For any object $\square_{\kappa\varepsilon}$ given in the original (R, U, ε)-variables, we denote the corresponding blown-up object by $\bar{\square}_{\kappa}$. Moreover, in chart K_i, that object will be denoted by $\square_{\kappa_i}$.

Lemma 1. *The change-of-coordinates transformation $\mathcal{K}_{12}$ between charts K_1 and K_2 is given by*

$$\mathcal{K}_{12} : (\rho_1, u_1, \varepsilon_1) \mapsto \left(\rho_2 r_2, \frac{u_2}{r_2^2}, \frac{1}{r_2^2}\right);$$

its inverse $\mathcal{K}_{21} = \mathcal{K}_{12}^{-1}$ reads

$$\mathcal{K}_{21} : (r_2, u_2, \rho_2) \mapsto \left(\frac{1}{\sqrt{\varepsilon_1}}, \frac{u_1}{\varepsilon_1}, \rho_1\sqrt{\varepsilon_1}\right).$$

We will first consider the dynamics in the "rescaling" chart K_2; then, we will study the flow in the "phase-directional" chart K_1. In particular, the latter will allow us to describe the transition between the "inner" and "outer" regions, which correspond to regimes $\mathcal{R}_2$ and $\mathcal{R}_3$, respectively, as defined in Section 3.

4.2. Dynamics in chart K_2

In chart K_2, the blow-up transformation defined in (24) is given by (26); substituting into Equation (23), we find

$$r_2' = \kappa\rho_2^4(u_2 + \mathcal{P})\frac{(u_2+1)^2 + \Lambda\rho_2^2 r_2^2 u_2^2}{(u_2+1)(u_2+\frac{1}{c})}\left[\tilde{\mu}(u_2+1) - \left(u_2 + \tilde{d}\rho_2\right)r_2\right], \tag{27a}$$

$$u_2' = \rho_2^4\left\{\tilde{b}\rho_2^2(u_2+1)^2 + \Theta r_2^2 u_2^2 - u_2\left[(u_2+1)^2 + \Lambda\rho_2^2 r_2^2 u_2^2\right]\right\}, \tag{27b}$$

$$\rho_2' = 0. \tag{27c}$$

By dividing out a factor of ρ_2^4 from the right-hand sides in Equation (27), we obtain the desingularised dynamics in chart K_2:

$$r_2' = \kappa(u_2+\mathcal{P})\frac{(u_2+1)^2+\Lambda\rho_2^2r_2^2u_2^2}{(u_2+1)(u_2+\frac{1}{c})}\big[\tilde{\mu}(u_2+1)-\big(u_2+\tilde{d}\rho_2\big)r_2\big], \tag{28a}$$

$$u_2' = \tilde{b}\rho_2^2(u_2+1)^2+\Theta r_2^2u_2^2-u_2\big[(u_2+1)^2+\Lambda\rho_2^2r_2^2u_2^2\big], \tag{28b}$$

$$\rho_2' = 0, \tag{28c}$$

which is a slow-fast system in standard form, with singular perturbation parameter κ; correspondingly, the variable r_2 is slow, while u_2 is fast. We observe that K_2 corresponds precisely to regime $\mathcal{R}_2$, as Equation (28) is equivalent to (18), with $(R_2,U_2)=(r_2,u_2)$, $\varepsilon=\rho_2^2$, and the (trivial) equation $\rho_2'=0$ appended. Hence, the geometric singular perturbation analysis in chart K_2 proceeds as in Section 3.2; the relevant dynamics in blown-up space is again illustrated in Fig. 6. In particular, it follows that the geometry of Equation (28) described in Section 3.2 is valid on compact domains in K_2.

We first consider the flow of Equation (28) in the invariant plane $\{\rho_2=0\}$, which is governed by

$$r_2' = \kappa(u_2+\mathcal{P})\frac{u_2+1}{u_2+\frac{1}{c}}\big[\tilde{\mu}(u_2+1)-u_2r_2\big], \tag{29a}$$

$$u_2' = \Theta r_2^2u_2^2-u_2(u_2+1)^2, \tag{29b}$$

$$\rho_2' = 0. \tag{29c}$$

Equation (29) is again a slow-fast system in standard form, with singular perturbation parameter κ; correspondingly, the variable r_2 is slow, while u_2 is fast. The corresponding layer problem reads

$$r_2' = 0, \tag{30a}$$

$$u_2' = \Theta r_2^2u_2^2-u_2(u_2+1)^2, \tag{30b}$$

$$\rho_2' = 0. \tag{30c}$$

It follows immediately from Section 3.2 that the critical manifold for Equation (30) consists of the three branches $\mathcal{S}_{0_2}^{a-}$, $\mathcal{S}_{0_2}^{r}$, and $\mathcal{S}_{0_2}^{a+}$; the former equals a segment of the r_2-axis, and is normally attracting under the flow of (30). The branches $\mathcal{S}_{0_2}^{r}$ and $\mathcal{S}_{0_2}^{a+}$ are separated by the fold point C_{0_2} at which hyperbolicity is lost; $\mathcal{S}_{0_2}^{r}$ is normally repelling, while $\mathcal{S}_{0_2}^{a+}$ is normally attracting, outside of a neighbourhood of that point. See again Fig. 6 for an illustration; here, the notation $\square_{0_2}$ in chart K_2 corresponds to $\square_{00_2}$ in regime $\mathcal{R}_2$.

4.3. Dynamics in chart K_1

In chart K_1, the blow-up transformation defined in Equation (24) is given by (25). Substituting into Equation (23), dividing out a factor of ρ_1^4 from the resulting equations, as before, and setting

$$F_1(\rho_1,u_1,\varepsilon_1) = (u_1+\mathcal{P}\varepsilon_1)\frac{(u_1+\varepsilon_1)^2+\Lambda\rho_1^2u_1^2}{(u_1+\varepsilon_1)(u_1+\frac{\varepsilon_1}{c})}\Big[\tilde{\mu}\varepsilon_1^{\frac{1}{2}}(u_1+\varepsilon_1)-\Big(u_1+\tilde{d}\rho_1\varepsilon_1^{\frac{3}{2}}\Big)\Big],$$

we obtain the system

$$\rho_1' = \kappa\rho_1F_1(\rho_1,u_1,\varepsilon_1), \tag{31a}$$

$$u_1' = \tilde{b}\rho_1^2\varepsilon_1^2(u_1+\varepsilon_1)^2+\Theta u_1^2-u_1\big[(u_1+\varepsilon_1)^2+\Lambda\rho_1^2u_1^2\big]-2\kappa u_1F_1(\rho_1,u_1,\varepsilon_1), \tag{31b}$$

$$\varepsilon_1' = -2\kappa\varepsilon_1F_1(\rho_1,u_1,\varepsilon_1), \tag{31c}$$

which is a slow-fast system with singular perturbation parameter κ; correspondingly, the variables ρ_1 and ε_1 are slow, while u_1 is fast.

Remark 14. *A priori*, it may seem that the denominator $(u_1+\varepsilon_1)(u_1+\frac{\varepsilon_1}{c})$ in $F_1(\rho_1,u_1,\varepsilon_1)$ may cause non-uniformity in the limit as $(u_1,\varepsilon_1)\to(0,0)$. However, one can show that F_1 vanishes to the order $\mathcal{O}(2)$ at $(u_1,\varepsilon_1)=(0,0)$, which is sufficient for our purposes.

Setting $\kappa=0$ in Equation (31) gives the layer problem

$$\rho_1' = 0, \tag{32a}$$
$$u_1' = \tilde{b}\rho_1^2\varepsilon_1^2(u_1+\varepsilon_1)^2 + \Theta u_1^2 - u_1\big[(u_1+\varepsilon_1)^2 + \Lambda\rho_1^2u_1^2\big], \tag{32b}$$
$$\varepsilon_1' = 0; \tag{32c}$$

the corresponding critical manifold $\mathcal{S}_{0_1}$ is the hypersurface in $(\rho_1,u_1,\varepsilon_1)$-space that is defined by

$$\tilde{b}\rho_1^2\varepsilon_1^2(u_1+\varepsilon_1)^2 + \Theta u_1^2 - u_1\big[(u_1+\varepsilon_1)^2 + \Lambda\rho_1^2u_1^2\big] = 0. \tag{33}$$

Rather than attempting a global description of $\mathcal{S}_{0_1}$, we will restrict ourselves to the two invariant hyperplanes $\{\rho_1=0\}$ and $\{\varepsilon_1=0\}$ for Equation (31), which will allow us to infer the geometry of $\mathcal{S}_{0_1}$ for either ρ_1 or ε_1 small. The flow in the plane $\{\rho_1=0\}$ is governed by

$$u_1' = \Theta u_1^2 - u_1(u_1+\varepsilon_1)^2 - 2\kappa u_1F_1(0,u_1,\varepsilon_1), \tag{34a}$$
$$\varepsilon_1' = -2\kappa\varepsilon_1F_1(0,u_1,\varepsilon_1), \tag{34b}$$

with

$$F_1(0,u_1,\varepsilon_1) = (u_1+\mathcal{P}\varepsilon_1)\frac{u_1+\varepsilon_1}{u_1+\frac{\varepsilon_1}{c}}\Big[\tilde{\mu}\varepsilon_1^{\frac{1}{2}}(u_1+\varepsilon_1) - u_1\Big].$$

(One can again show that $F_1(0,u_1,\varepsilon_1)$ vanishes to the order $\mathcal{O}(2)$ at $(u_1,\varepsilon_1)=(0,0)$; recall Remark 14.) Setting $\kappa=0$ in Equation (34), we obtain the layer problem

$$u_1' = \Theta u_1^2 - u_1(u_1+\varepsilon_1)^2, \tag{35a}$$
$$\varepsilon_1' = 0. \tag{35b}$$

The critical manifold of Equation (35), which is denoted by $\hat{\mathcal{S}}_{0_1}$, is defined by $u_1\big[\Theta u_1-(u_1+\varepsilon_1)^2\big]=0$; it consists of a normally attracting left branch $\hat{\mathcal{S}}_{0_1}^{a-}$ corresponding to the invariant line $\{u_1=0\}$ with ε_1 positive, a normally repelling middle branch $\hat{\mathcal{S}}_{0_1}^{r}$ that corresponds to $u_1\in(0,\frac{\Theta}{4})$, and a normally attracting right branch $\hat{\mathcal{S}}_{0_1}^{a+}$ corresponding to $u_1\in(\frac{\Theta}{4},\Theta]$. The branches $\hat{\mathcal{S}}_{0_1}^{r}$ and $\hat{\mathcal{S}}_{0_1}^{a+}$ are separated by the fold point C_{0_1}; the equilibrium E_{0_1}, which is easily obtained from (33), lies on $\hat{\mathcal{S}}_{0_1}^{r}$ due to our assumptions on the parameters μ and Θ, while $\hat{\mathcal{S}}_{0_1}^{a-}$ and $\hat{\mathcal{S}}_{0_1}^{r}$ intersect in the origin $\hat{P}_1:(0,0,0)$. (We note that, clearly, all three branches of $\hat{\mathcal{S}}_{0_1}$ are intersections of $\mathcal{S}_{0_1}$ with the plane $\{\rho_1=0\}$.) From the corresponding reduced problem, we see that ε_1 increases above E_{0_1} on $\hat{\mathcal{S}}_{0_1}^{r}$ and on $\hat{\mathcal{S}}_{0_1}^{a+}$, while it decreases below E_{0_1} on $\hat{\mathcal{S}}_{0_1}^{r}$ and on $\hat{\mathcal{S}}_{0_1}^{a-}$. Hence, orbits follow the slow manifold $\hat{\mathcal{S}}_{0_1}^{a+}$ until they reach the fold point at C_{0_1}, where they jump to the point $B_{0_1}:\big(0,0,\frac{\Theta}{4}\big)\in\hat{\mathcal{S}}_{0_1}^{a-}$. The geometry in $\{\rho_1=0\}$ is summarised in Fig. 9.

In the invariant plane $\{\varepsilon_1=0\}$, $F_1(\rho_1,u_1,0)=-u_1^2\big(1+\Lambda\rho_1^2\big)$ implies

$$\rho_1' = -\kappa\rho_1u_1^2\big(1+\Lambda\rho_1^2\big), \tag{36a}$$
$$u_1' = u_1^2\big[\Theta-u_1\big(1+\Lambda\rho_1^2\big)\big] + 2\kappa u_1^3\big(1+\Lambda\rho_1^2\big), \tag{36b}$$

which, for $\kappa=0$, yields the layer problem

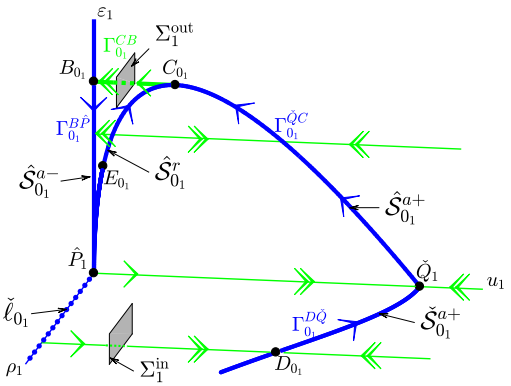

Fig. 9. Geometry in $\{\rho_1 = 0\}$ and $\{\varepsilon_1 = 0\}$, for $\kappa = 0$, in chart K_1: reduced flow (solid blue), layer dynamics (solid green), and equilibrium E_{0_1}.

$$\rho_1' = 0, \tag{37a}$$

$$u_1' = u_1^2\big[\Theta - u_1\big(1 + \Lambda\rho_1^2\big)\big]. \tag{37b}$$

The critical manifold for Equation (37), which is denoted by $\check{\mathcal{S}}_{0_1}$, is defined by $u_1^2\big[\Theta - u_1\big(1+\Lambda\rho_1^2\big)\big] = 0$. A straightforward calculation shows that $\check{\mathcal{S}}_{0_1}$ consists of a right attracting branch $\check{\mathcal{S}}_{0_1}^{a+}$ corresponding to the invariant curve $u_1 = \frac{\Theta}{1+\Lambda\rho_1^2}$ and the non-hyperbolic line $\check{\ell}_{0_1}$, given by $\{u_1 = 0\}$. Both branches of $\check{\mathcal{S}}_{0_1}$ are intersections of the critical manifold $\mathcal{S}_{0_1}$ for Equation (32) with the plane $\{\varepsilon_1 = 0\}$. From the corresponding reduced problem, we find that ρ_1 is decreasing on $\check{\mathcal{S}}_{0_1}^{a+}$. Finally, the curves $\check{\mathcal{S}}_{0_1}^{a+}$ and $\hat{\mathcal{S}}_{0_1}^{a+}$ intersect on the u_1-axis at the point $\check{Q}_1 : (0, \Theta, 0)$; see again Fig. 9 for an illustration.

Remark 15. We emphasise that the critical manifold $\hat{S}_{0_1}$ and the fold point C_{0_1} for Equation (35) were already identified in chart K_2, and that they are hence merely recovered in K_1.

We may summarise the above discussion as follows:

Lemma 2. *For ρ_1 or ε_1 sufficiently small, the critical manifold $\mathcal{S}_{0_1}$ that is defined by Equation (33) has the following properties:*

i. The manifold $\mathcal{S}_{0_1} = \mathcal{S}_{0_1}^{a-} \cup \mathcal{S}_{0_1}^{r} \cup \mathcal{F}_{0_1}^{C} \cup \mathcal{S}_{0_1}^{a+}$ is smooth away from the line $\check{\ell}_{0_1}$.

ii. The manifold $\mathcal{S}_{0_1}$ has a folded structure; specifically, it is divided by the fold curve $\mathcal{F}_{0_1}^{C}$ into two branches $\mathcal{S}_{0_1}^{r}$ and $\mathcal{S}_{0_1}^{a+}$, whereas the branches $\mathcal{S}_{0_1}^{a-}$ and $\mathcal{S}_{0_1}^{r}$ intersect cusp-like along $\check{\ell}_{0_1}$.

iii. The branches $\mathcal{S}_{0_1}^{a-}$ and $\mathcal{S}_{0_1}^{a+}$ are attracting under the layer flow of Equation (32), while the branch $\mathcal{S}_{0_1}^{r}$ is repelling.

iv. The restriction of $\mathcal{S}_{0_1}^{a-}$, $\mathcal{S}_{0_1}^{r}$, and $\mathcal{S}_{0_1}^{a+}$ to the invariant hyperplane $\{\rho_1 = 0\}$ corresponds to $\hat{\mathcal{S}}_{0_1}^{a-}$, $\hat{\mathcal{S}}_{0_1}^{r}$, and $\hat{\mathcal{S}}_{0_1}^{a+}$, respectively; correspondingly, the fold curve $\mathcal{F}_{0_1}^{C}$ reduces to the point C_{0_1}.

v. In the invariant hyperplane $\{\varepsilon_1 = 0\}$, $\mathcal{S}_{0_1}^{a-}$ and $\mathcal{S}_{0_1}^{r}$ coalesce into $\check{\ell}_{0_1}$, while $\mathcal{S}_{0_1}^{a+}$ corresponds to $\check{\mathcal{S}}_{0_1}^{a+}$ in that limit.

Proof. Outside of a neighbourhood of the line $\check{\ell}_{0_1}$, the above assertions follow from the Implicit Function Theorem, in combination with the structural stability of folds; see [13] and the references therein for details. The geometry of the manifold $\mathcal{S}_{0_1}$ near $\check{\ell}_{0_1}$, and the corresponding dynamics of Equation (31), will be considered in Section 4.4 below. □

For future reference, we define the sections Σ_1^{in} and Σ_1^{out} for the flow of Equation (31) as

$$\Sigma_1^{\text{in}} := \left\{ \left(\rho_1, \tfrac{\Theta}{4}, \varepsilon_1\right) \,\middle|\, \rho_1 - \tfrac{1}{2\sqrt{\Theta b}} \in [\rho_*, \rho^*], \varepsilon_1 \in [\varepsilon_*, \varepsilon^*] \right\} \quad \text{and} \tag{38a}$$

$$\Sigma_1^{\text{out}} := \left\{ \left(\rho_1, \tfrac{\Theta}{8}, \varepsilon_1\right) \,\middle|\, \rho_1 \in [\rho_*, \rho^*], \varepsilon_1 - \tfrac{\Theta}{4} \in [\varepsilon_*, \varepsilon^*] \right\}, \tag{38b}$$

respectively; see Fig. 9. (Here, ρ_*, ρ^*, ε_*, and ε^* are suitably chosen constants.)

The situation in chart K_1 can be summarised as follows: the segment $\Gamma_{0_1}^{D\check{Q}}$ of the singular orbit is initialised close to a point D_{0_1} which will be specified in chart K_4 in the following section; the orbit is attracted to $\check{\mathcal{S}}_{0_1}^{a+}$ and then follows the slow flow thereon until it reaches the point $\check{Q}_1$. The continuation of $\Gamma_{0_1}^{D\check{Q}}$ past $\check{Q}_1$ is given by the orbit $\Gamma_{0_1}^{\check{Q}C}$ along the slow flow on $\hat{\mathcal{S}}_{0_1}^{a+}$ to the fold point C_{0_1}, where the orbit $\Gamma_{0_1}^{CB}$ represents the jump along the fast flow to the point B_{0_1} on $\hat{\mathcal{S}}_{0_1}^{a-}$; the orbit $\Gamma_{0_1}^{B\hat{P}}$ then follows the slow flow on $\hat{\mathcal{S}}_{0_1}^{a-}$ to the origin $\hat{P}_1$, which is still a non-hyperbolic steady state for (31). The continuation of the orbit is located on the degenerate (non-hyperbolic) line $\check{\ell}_{0_1}$; to resolve that degeneracy, we require a further blow-up transformation, which is introduced in the subsequent subsection. The geometry in the hyperplanes $\{\rho_1 = 0\}$ and $\{\varepsilon_1 = 0\}$ in chart K_1 is illustrated in Fig. 9.

4.4. Blow-up of the non-hyperbolic line $\check{\ell}_{0_1}$

To analyse the dynamics in a neighbourhood of the non-hyperbolic line $\check{\ell}_{0_1}$ recovered in chart K_1, we introduce the quasi-homogeneous, cylindrical blow-up transformation

$$\rho_1 = \bar{r}, \quad u_1 = \delta^2 \bar{u}, \quad \text{and} \quad \varepsilon_1 = \delta \bar{\varepsilon}, \tag{39}$$

with $\bar{r} \in \mathbb{R}^+$, $(\bar{u}, \bar{\varepsilon}) \in \mathbb{S}^1$, and $\delta \in [0, \delta_0]$, for δ_0 positive and small; in other words, the line $\check{\ell}_{0_1}$ is blown up to the cylinder $\mathbb{R}^+ \times \mathbb{S}^1 \times \{0\}$. We emphasise that this second blow-up is performed entirely in chart K_1.

The vector field that is induced by Equation (31) is studied in two coordinate charts K_3 and K_4, which are obtained for $\bar{\varepsilon} = 1$ and $\bar{u} = 1$ in (39), respectively; see again [3,14] for details. Hence, we have

$$\rho_1 = r_3, \quad u_1 = \delta_3^2 u_3, \quad \text{and} \quad \varepsilon_1 = \delta_3 \tag{40}$$

and

$$\rho_1 = r_4, \quad u_1 = \delta_4^2, \quad \text{and} \quad \varepsilon_1 = \delta_4 \varepsilon_4, \tag{41}$$

respectively, for the coordinates in these charts. Intuitively, chart K_3 covers the top of the cylinder $\mathbb{R}^+ \times \mathbb{S}^1 \times \{0\}$ corresponding to $\bar{\varepsilon}$ positive, while the flow in a neighbourhood of the front of that cylinder, with $\bar{u}$ positive, is described in chart K_4; cf. again Fig. 12 below.

Lemma 3. *The change-of-coordinates transformation $\mathcal{K}_{34}$ between charts K_3 and K_4 is given by*

$$\mathcal{K}_{34} : (r_3, u_3, \delta_3) \mapsto \left(r_4, \frac{1}{\varepsilon_4^2}, \delta_4 \varepsilon_4\right);$$

its inverse $\mathcal{K}_{43} = \mathcal{K}_{34}^{-1}$ reads

$$\mathcal{K}_{43} : (r_4, \delta_4, \varepsilon_4) \mapsto \left(r_3, \sqrt{u_3}\delta_3, \frac{1}{\sqrt{u_3}}\right).$$

As will become clear in the following, chart K_3 covers the transition between regimes $\mathcal{R}_1$ and $\mathcal{R}_2$, while the transition between $\mathcal{R}_1$ and $\mathcal{R}_3$ is naturally described in chart K_4; both charts provide sufficient overlap for matching to be accomplished between the respective scaling regimes.

4.5. Dynamics in chart K_3

In chart K_3, the blow-up transformation defined by $\bar{\varepsilon} = 1$ in Equation (39) is given as in (40). Substituting into Equation (31), dividing out the factor δ_3^2 from the resulting equations, and defining

$$F_3(r_3, u_3, \delta_3) = F_1(r_3, \delta_3^2 u_3, \delta_3)\delta_3^{-2} = \delta_3^{\frac{1}{2}}(\delta_3 u_3 + \mathcal{P})\frac{(\delta_3 u_3 + 1)^2 + \Lambda r_3^2 \delta_3^2 u_3^2}{(\delta_3 u_3 + 1)(\delta_3 u_3 + \frac{1}{c})} \times \Big[\tilde{\mu}(\delta_3 u_3 + 1) - \Big(\delta_3^{\frac{1}{2}} u_3 + \tilde{d} r_3\Big)\Big],$$

we obtain the system

$$r_3' = \kappa r_3 F_3(r_3, u_3, \delta_3), \tag{42a}$$
$$u_3' = \tilde{b} r_3^2(\delta_3 u_3 + 1)^2 + \Theta u_3^2 - u_3\big[(\delta_3 u_3 + 1)^2 + \Lambda r_3^2 \delta_3^2 u_3^2\big] + 2\kappa u_3 F_3(r_3, u_3, \delta_3), \tag{42b}$$
$$\delta_3' = -2\kappa \delta_3 F_3(r_3, u_3, \delta_3), \tag{42c}$$

which is a slow-fast system with singular perturbation parameter κ; correspondingly, the variables r_3 and δ_3 are slow, while u_3 is fast. Here, the prime now denotes differentiation with respect to a new independent variable. For $\kappa = 0$ in (42), one obtains the layer problem

$$r_3' = 0, \tag{43a}$$
$$u_3' = \tilde{b} r_3^2(\delta_3 u_3 + 1)^2 + \Theta u_3^2 - u_3\big[(\delta_3 u_3 + 1)^2 + \Lambda r_3^2 \delta_3^2 u_3^2\big], \tag{43b}$$
$$\delta_3' = 0. \tag{43c}$$

The corresponding critical manifold $\mathcal{S}_{0_3}$ is the hypersurface in (r_3, u_3, δ_3)-space that is defined by

$$\tilde{b} r_3^2(\delta_3 u_3 + 1)^2 + \Theta u_3^2 - u_3\big[(\delta_3 u_3 + 1)^2 + \Lambda r_3^2 \delta_3^2 u_3^2\big] = 0. \tag{44}$$

The flow of Equation (42) in the invariant plane $\{r_3 = 0\}$ is governed by

$$u_3' = \Theta u_3^2 - u_3(\delta_3 u_3 + 1)^2 + 2\kappa u_3 F_3(0, u_3, \delta_3), \tag{45a}$$
$$\delta_3' = -2\kappa \delta_3 F_3(0, u_3, \delta_3), \tag{45b}$$

with

$$F_3(0, u_3, \delta_3) = \delta_3^{\frac{1}{2}}(\delta_3 u_3 + \mathcal{P})\frac{\delta_3 u_3 + 1}{\delta_3 u_3 + \frac{1}{c}}\Big[\tilde{\mu}(\delta_3 u_3 + 1) - \delta_3^{\frac{1}{2}} u_3\Big],$$

which is again a slow-fast system with respect to κ; correspondingly, the variable δ_3 is slow, while u_3 is a fast variable. Setting $\kappa = 0$, we obtain the layer problem

$$u_3' = \Theta u_3^2 - u_3(\delta_3 u_3 + 1)^2, \tag{46a}$$
$$\delta_3' = 0. \tag{46b}$$

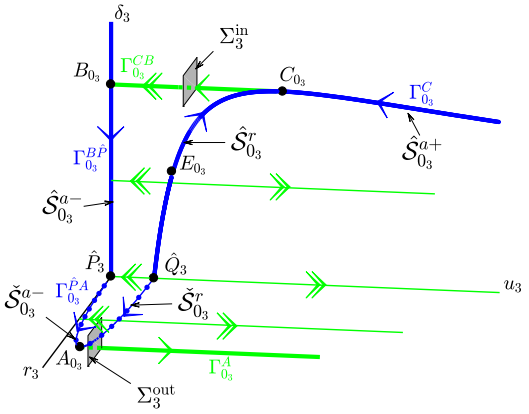

Fig. 10. Geometry in $\{r_3 = 0\}$ and $\{\delta_3 = 0\}$, for $\kappa = 0$, in chart K_3: reduced flow (solid blue), layer dynamics (solid green), and equilibrium E_{0_3}.

The critical manifold in the plane $\{r_3 = 0\}$, which we denote by $\hat{\mathcal{S}}_{0_3}$, is defined by $u_3\left[\Theta u_3 - (\delta_3 u_3 + 1)^2\right] = 0$. It consists of an attracting left branch $\hat{\mathcal{S}}^{a-}_{0_3}$ – the δ_3-axis, a repelling middle branch $\hat{\mathcal{S}}^{r}_{0_3}$, and an attracting right branch $\hat{\mathcal{S}}^{a+}_{0_3}$. The branches $\hat{\mathcal{S}}^{r}_{0_3}$ and $\hat{\mathcal{S}}^{a+}_{0_3}$ are separated by a fold point at C_{0_3}; here, we note that the equilibrium E_{0_3} lies in $\hat{\mathcal{S}}^{r}_{0_3}$. Moreover, $\hat{\mathcal{S}}^{a-}_{0_3}$ and $\hat{\mathcal{S}}^{r}_{0_3}$ intersect the u_3-axis in the points $\hat{P}_3 : (0,0,0)$ and $\hat{Q}_3 : \left(0, \frac{1}{\Theta}, 0\right)$, respectively. All three branches of $\hat{\mathcal{S}}_{0_3}$ are intersections of $\mathcal{S}_{0_3}$ with the plane $\{r_3 = 0\}$. From the corresponding reduced problem, we conclude that δ_3 is increasing on $\hat{\mathcal{S}}^{r}_{0_3}$ above E_{0_3} and on $\hat{\mathcal{S}}^{a+}_{0_3}$, while it is decreasing on $\hat{\mathcal{S}}^{r}_{0_3}$ below E_{0_3} and on $\hat{\mathcal{S}}^{a-}_{0_3}$. Hence, orbits follow the slow manifold $\hat{\mathcal{S}}^{a+}_{0_3}$ until they reach the fold point C_{0_3}, where they jump to the point $B_{0_3} \in \hat{\mathcal{S}}^{a-}_{0_3}$.

Next, we consider the flow of Equation (42) in the invariant plane $\{\delta_3 = 0\}$, which is governed by

$$r_3' = 0, \tag{47a}$$

$$u_3' = \tilde{b} r_3^2 + \Theta u_3^2 - u_3. \tag{47b}$$

The corresponding critical manifold, which is denoted by $\check{\mathcal{S}}_{0_3}$, is defined by $\tilde{b} r_3^2 + \Theta u_3^2 - u_3 = 0$; it consists of a left attracting branch $\check{\mathcal{S}}^{a-}_{0_3}$ corresponding to $u_3 \in [0, \frac{1}{2\Theta})$ and a right repelling branch $\check{\mathcal{S}}^{a+}_{0_3}$ which is obtained for $u_3 \in (\frac{1}{2\Theta}, \frac{1}{\Theta}]$. The two branches are separated by the fold point A_{0_3}. Both branches are intersections of $\mathcal{S}_{0_3}$ with the plane $\{\delta_3 = 0\}$. The geometry in chart K_3 is summarised in Fig. 10.

Remark 16. The manifolds $\check{\mathcal{S}}_{0_3}$ and $\hat{\mathcal{S}}_{0_3}$ correspond precisely to the critical manifolds $\mathcal{S}_{00_1}$ and $\mathcal{S}_{00_2}$ uncovered in regimes $\mathcal{R}_1$ and $\mathcal{R}_2$, respectively. Hence, chart K_3 covers the transition between those two regimes, as claimed.

Due to $F_3(r_3, u_3, 0) = 0$, the reduced flow with respect to κ in $\{\delta_3 = 0\}$ is degenerate, in that it vanishes identically; hence, A_{0_3} is not a jump point in the classical sense of [14]. However, the equivalent of A_{0_3} in regime $\mathcal{R}_1$, denoted by A_{00_1} in Section 3.1, is, which allows for a description of the passage past A_{0_3} by recourse to $\mathcal{R}_1$; see also the proof of Lemma 10 below.

Remark 17. Alternatively, one may note that, for δ_3 positive and small, the factor $\left[\tilde{\mu}(\delta_3 u_3 + 1) - \left(\delta_3^{\frac{1}{2}} u_3 + \tilde{d} r_3\right)\right] = \tilde{\mu} - \tilde{d} r_3 - u_3 \delta_3^{\frac{1}{2}}\left(1 - \tilde{\mu}\delta_3^{\frac{1}{2}}\right)$ in the definition of F_3 is positive due to our choice of μ and d, which implies $\frac{\tilde{\mu}}{\tilde{d}} > \left(2\sqrt{\Theta\tilde{b}}\right)^{-1}$. Hence, $r_3' > 0$ for $r_3 < \left(2\sqrt{\Theta\tilde{b}}\right)^{-1}$, *i.e.*, the reduced flow in r_3 is directed towards A_{0_3}: orbits follow the corresponding sheet $\mathcal{S}^{a-}_{0_3}$ of S_{0_3} until they reach the fold curve $\mathcal{F}^{A}_{0_3}$ and then jump away under the layer flow of Equation (43); recall Remark 7. (The corresponding touch-down point is not visible in chart K_3.)

We conclude with the following result, the proof of which is analogous to that of Lemma 2:

Lemma 4. *For r_3 or δ_3 sufficiently small, the critical manifold $\mathcal{S}_{0_3}$ that is defined by Equation (44) has the following properties:*

i. The manifold $\mathcal{S}_{0_3} = \mathcal{S}_{0_3}^{a-} \cup \mathcal{F}_{0_3}^{A} \cup \mathcal{S}_{0_3}^{r} \cup \mathcal{F}_{0_3}^{C} \cup \mathcal{S}_{0_3}^{a+}$ is smooth.

ii. The manifold $\mathcal{S}_{0_3}$ has a folded structure; in particular, the branches $\mathcal{S}_{0_3}^{a-}$ and $\mathcal{S}_{0_3}^{r}$ are separated by the fold curve $\mathcal{F}_{0_3}^{A}$, while $\mathcal{S}_{0_3}^{r}$ and $\mathcal{S}_{0_3}^{a+}$ are separated by the fold curve $\mathcal{F}_{0_3}^{C}$.

iii. The branches $\mathcal{S}_{0_3}^{a-}$ and $\mathcal{S}_{0_3}^{a+}$ are attracting under the layer flow of Equation (43), while the branch $\mathcal{S}_{0_3}^{r}$ is repelling.

iv. The restriction of $\mathcal{S}_{0_3}^{a-}$, $\mathcal{S}_{0_3}^{r}$, and $\mathcal{S}_{0_3}^{a+}$ to the invariant hyperplane $\{r_3 = 0\}$ corresponds to $\hat{\mathcal{S}}_{0_3}^{a-}$, $\hat{\mathcal{S}}_{0_3}^{r}$, and $\hat{\mathcal{S}}_{0_3}^{a+}$, respectively. Correspondingly, the fold curve $F_{0_3}^{C}$ intersects $\{r_3 = 0\}$ in the point C_{0_3}.

v. In the invariant hyperplane $\{\delta_3 = 0\}$, $\mathcal{S}_{0_3}^{a-}$ and $\mathcal{S}_{0_3}^{r}$ reduce to $\check{\mathcal{S}}_{0_3}^{a-}$ and $\check{\mathcal{S}}_{0_3}^{r}$, respectively. The fold curve $\mathcal{F}_{0_3}^{A}$ intersects $\{\delta_3 = 0\}$ in the point A_{0_3}.

As in Section 4.3, we introduce two sections Σ_3^{in} and Σ_3^{out} for the flow of Equation (42) as

$$\Sigma_3^{\text{in}} := \left\{ (r_3, u_3, \delta_3) \,\middle|\, r_3 \in [r_*, r^*], u_3 - \tfrac{2}{\Theta} \in [u_*, u^*], \delta_3 - \tfrac{\Theta}{4} \in [\delta_*, \delta^*] \right\} \quad \text{and} \tag{48a}$$

$$\Sigma_3^{\text{out}} := \left\{ (r_3, \tfrac{1}{\Theta}, \delta_3) \,\middle|\, r_3 - \tfrac{1}{2\sqrt{\Theta \tilde{b}}} \in [r_*, r^*], \delta_3 \in [\delta_*, \delta^*] \right\}, \tag{48b}$$

respectively, where r_*, r^*, u_*, u^*, δ_*, and δ^* are suitably chosen constants, as before. Here, we note that Σ_3^{in} is equivalent to the section Σ_1^{out} defined in (38) via the change-of-coordinates transformation in (40), while Σ_3^{out} is defined directly in chart K_3.

In summary, the segment $\Gamma_{0_3}^{C}$ of the singular orbit follows the slow flow on $\hat{\mathcal{S}}_{0_3}^{a+}$ to the fold point C_{0_3}; the orbit $\Gamma_{0_3}^{CB}$ represents the jump along the fast flow to the point B_{0_3}. The segment $\Gamma_{0_3}^{B\hat{P}}$ then follows the slow flow on $\hat{\mathcal{S}}_{0_3}^{a-}$ until it reaches the origin $\hat{P}_3$, continuing with the curve of equilibria $\Gamma_{0_3}^{\hat{P}A}$ that corresponds to the segment of $\check{\mathcal{S}}_{0_3}^{a-}$ between $\hat{P}_3$ and the fold point A_{0_3}; finally, the orbit jumps along the fast flow to the right for u_3 large. We label the corresponding segment by $\Gamma_{0_3}^{A}$; see Fig. 10 for an illustration. The large-u_3 dynamics of Equation (42) is then naturally studied in chart K_4.

4.6. Dynamics in chart K_4

In chart K_4, the blow-up transformation defined by $\bar{u}_1 = 1$ in Equation (39) is given as in (41). Substituting into Equation (31), dividing out a factor of δ_4^2, and defining

$$F_4(r_4, \delta_4, \varepsilon_4) = F_1(r_4, \delta_4^2, \delta_4 \varepsilon_4)\delta_4^{-2} = \delta_4^{\frac{1}{2}}(\delta_4 + \mathcal{P}\varepsilon_4)\frac{(\delta_4 + \varepsilon_4)^2 + \Lambda r_4^2 \delta_4^2}{(\delta_4 + \varepsilon_4)(\delta_4 + \frac{\varepsilon_4}{c})}$$
$$\times \left[\tilde{\mu} \varepsilon_4^{\frac{1}{2}}(\delta_4 + \varepsilon_4) - \left(\delta_4^{\frac{1}{2}} + \tilde{d} r_4 \varepsilon_4^{\frac{3}{2}} \right) \right],$$

we obtain the simplified system

$$r_4' = \kappa r_4 F_4(r_4, \delta_4, \varepsilon_4), \tag{49a}$$

$$\delta_4' = \frac{1}{2}\delta_4 \left\{ \tilde{b} r_4^2 \varepsilon_4^2 (\delta_4 + \varepsilon_4)^2 + \Theta - \left[(\delta_4 + \varepsilon_4)^2 + \Lambda r_4^2 \delta_4^2 \right] \right\} - \kappa \delta_4 F_4(r_4, \delta_4, \varepsilon_4), \tag{49b}$$

$$\varepsilon_4' = -\frac{1}{2}\varepsilon_4 \left\{ \tilde{b} r_4^2 \varepsilon_4^2 (\delta_4 + \varepsilon_4)^2 + \Theta - \left[(\delta_4 + \varepsilon_4)^2 + \Lambda r_4^2 \delta_4^2 \right] \right\} - \kappa \varepsilon_4 F_4(r_4, \delta_4, \varepsilon_4), \tag{49c}$$

which is a slow-fast system with singular perturbation parameter κ; correspondingly, the variable r_4 is slow, while δ_4 and ε_4 are fast. Here, the prime again denotes differentiation with respect to a new independent variable.

Remark 18. The denominator $(\delta_4+\varepsilon_4)(\delta_4+\frac{\varepsilon_4}{c})$ in $F_4(r_4,\delta_4,\varepsilon_4)$ may be expected to render the limit as $(\delta_4,\varepsilon_4)\to(0,0)$ in (49) non-uniform. However, F_4 again vanishes to the order $\mathcal{O}(2)$ at $(\delta_4,\varepsilon_4)=(0,0)$; recall Remark 14.

Setting $\kappa=0$ in (49), we obtain the layer problem

$$r_4' = 0, \tag{50a}$$
$$\delta_4' = \frac{1}{2}\delta_4\big\{\tilde{b}r_4^2\varepsilon_4^2(\delta_4+\varepsilon_4)^2+\Theta-\big[(\delta_4+\varepsilon_4)^2+\Lambda r_4^2\delta_4^2\big]\big\}, \tag{50b}$$
$$\varepsilon_4' = -\frac{1}{2}\varepsilon_4\big\{\tilde{b}r_4^2\varepsilon_4^2(\delta_4+\varepsilon_4)^2+\Theta-\big[(\delta_4+\varepsilon_4)^2+\Lambda r_4^2\delta_4^2\big]\big\}. \tag{50c}$$

The corresponding critical manifold $\mathcal{S}_{0_4}$ is the hypersurface in $(r_4,\delta_4,\varepsilon_4)$-space that is defined by

$$\tilde{b}r_4^2\varepsilon_4^2(\delta_4+\varepsilon_4)^2+\Theta-\big[(\delta_4+\varepsilon_4)^2+\Lambda r_4^2\delta_4^2\big]=0; \tag{51}$$

an additional line of equilibria is found for $\delta_4=0=\varepsilon_4$, i.e., on the r_4-axis.

Remark 19. Since δ_4 and ε_4 are fast variables outside of a neighbourhood of $\mathcal{S}_{0_4}$, Equation (49) is not a slow-fast system in standard form; details can be found in [13].

We consider the flow of Equation (50) in the invariant plane $\{\delta_4=0\}$, which is governed by

$$r_4' = 0, \tag{52a}$$
$$\varepsilon_4' = -\frac{1}{2}\varepsilon_4\big(\tilde{b}r_4^2\varepsilon_4^4+\Theta-\varepsilon_4^2\big). \tag{52b}$$

The corresponding critical manifold is defined by

$$\tilde{b}r_4^2\varepsilon_4^4+\Theta-\varepsilon_4^2=0;$$

it consists of a lower repelling branch $\check{\mathcal{S}}_{0_4}^r$ corresponding to $\varepsilon_4\in[\sqrt{\Theta},\sqrt{2\Theta})$ and an upper attracting branch $\check{\mathcal{S}}_{0_4}^{a-}$ with $\varepsilon_4\in(\sqrt{2\Theta},\infty)$, which are separated by the fold point A_{0_4}. We denote the line of additional equilibria on the r_4-axis by $\check{\ell}_{0_4}$; here, we emphasise that $\check{\ell}_{0_4}$ is attracting in $\{\delta_4=0\}$. All three branches are found in the intersection of $\mathcal{S}_{0_4}$ with the plane $\{\delta_4=0\}$. Orbits follow the slow manifold $\check{\mathcal{S}}_{0_4}^{a-}$ until they reach the fold point at A_{0_4}, where they jump forward to the point $\check{P}_4:\ \left(\frac{1}{2\sqrt{\Theta\tilde{b}}},0,0\right)\in\check{\ell}_{0_4}$.

In the invariant plane $\{\varepsilon_4=0\}$, Equation (49) reduces to

$$r_4' = -\kappa r_4\delta_4^2\big(1+\Lambda r_4^2\big), \tag{53a}$$
$$\delta_4' = \frac{1}{2}\delta_4\big[\Theta-\delta_4^2\big(1+\Lambda r_4^2\big)\big]+\kappa\delta_4^3\big(1+\Lambda r_4^2\big), \tag{53b}$$

as $F_4(r_4,\delta_4,0)=-\delta_4^2\big(1+\Lambda r_4^2\big)$ then. The corresponding layer problem is obtained for $\kappa=0$:

$$r_4' = 0, \tag{54a}$$
$$\delta_4' = \frac{1}{2}\delta_4\big[\Theta-\delta_4^2\big(1+\Lambda r_4^2\big)\big], \tag{54b}$$

which implies that the critical manifold satisfies $\Theta-\delta_4^2\big(1+\Lambda r_4^2\big)=0$. That manifold consists of an attracting branch $\check{\mathcal{S}}_{0_4}^{a+}$, which intersects the δ_4-axis in the point $\check{Q}_4=(0,\sqrt{\Theta},0)$; the line of equilibria on the r_4-axis, denoted again by $\check{\ell}_{0_4}$, is repelling in $\{\varepsilon_4=0\}$. Orbits starting close to $\check{P}_4\in\check{\ell}_{0_4}$ leave along the unstable manifold thereof and jump to the point $D_{0_4}:\ \Big(\frac{1}{2\sqrt{\Theta\tilde{b}}},\frac{2\Theta\sqrt{\tilde{b}}}{\sqrt{4\Theta\tilde{b}+\Lambda}},0\Big)$ in $\check{\mathcal{S}}_{0_4}^{a+}$; then, they follow the slow manifold $\check{\mathcal{S}}_{0_4}^{a+}$ until they reach the point $\check{Q}_4$. An illustration of the resulting geometry can be found in Fig. 11.

Similarly, in the invariant plane $\{r_4=0\}$, the flow of Equation (49) is governed by

$$\delta_4'=\frac{1}{2}\delta_4\big[\Theta-(\delta_4+\varepsilon_4)^2\big]-\kappa\delta_4F_4(0,\delta_4,\varepsilon_4), \tag{55a}$$

$$\varepsilon_4'=-\frac{1}{2}\varepsilon_4\big[\Theta-(\delta_4+\varepsilon_4)^2\big]-\kappa\varepsilon_4F_4(0,\delta_4,\varepsilon_4), \tag{55b}$$

where

$$F_4(0,\delta_4,\varepsilon_4)=\delta_4^{\frac{1}{2}}(\delta_4+\mathcal{P}\varepsilon_4)\frac{\delta_4+\varepsilon_4}{\delta_4+\frac{\varepsilon_4}{c}}\Big[\tilde{\mu}\varepsilon_4^{\frac{1}{2}}(\delta_4+\varepsilon_4)-\delta_4^{\frac{1}{2}}\Big].$$

(One can show that $\delta_4F_4(0,\delta_4,\varepsilon_4)$ and $\varepsilon_4F_4(0,\delta_4,\varepsilon_4)$ vanish to the order $\mathcal{O}(3)$ at $(\delta_4,\varepsilon_4)=(0,0)$; recall Remark 14.) Setting $\kappa=0$, we obtain the layer problem

$$\delta_4'=\frac{1}{2}\delta_4\big[\Theta-(\delta_4+\varepsilon_4)^2\big], \tag{56a}$$

$$\varepsilon_4'=-\frac{1}{2}\varepsilon_4\big[\Theta-(\delta_4+\varepsilon_4)^2\big]; \tag{56b}$$

the corresponding critical manifold, which is denoted by $\hat{\mathcal{S}}_{0_4}$, is defined by

$$\Theta-(\delta_4+\varepsilon_4)^2=0.$$

(The additional steady state which is located at the origin is attracting in the ε_4-direction, but repelling in the direction of δ_4; see our definition of $\check{\ell}_{0_4}$ above.) The manifold $\hat{\mathcal{S}}_{0_4}$ is, in fact, a line connecting the point $\check{Q}_4$ to the point $\hat{Q}_4:\ (0,0,\sqrt{\Theta})$; it consists of an attracting right segment $\hat{\mathcal{S}}_{0_4}^{a+}$ and a repelling left segment $\hat{\mathcal{S}}_{0_4}^{r}$ that exchange stability at the point C_{0_4}, which is not a genuine fold point in the coordinates of chart K_4. The corresponding equilibrium E_{0_4} lies in $\hat{\mathcal{S}}_{0_4}^{r}$; the reduced flow on $\hat{\mathcal{S}}_{0_4}^{r}$ is increasing above E_{0_4}, while it decreases below E_{0_4} until it reaches C_{0_4}.

Remark 20. Clearly, most of the objects described above have already been identified in other coordinate charts, viz. in K_1 and K_3. Our focus in this subsection is on the description of the flow past the line $\check{\ell}_{0_4}$; see Equation (57) below.

In conclusion, we have the following result, the proof of which is again analogous to that of Lemma 2:

Lemma 5. *For r_4, δ_4, or ε_4 sufficiently small, the critical manifold $\mathcal{S}_{0_4}$ that is defined by Equation (51) has the following properties:*

i. The manifold $\mathcal{S}_{0_4}=\mathcal{S}_{0_4}^{a-}\cup\mathcal{F}_{0_4}^{A}\cup\mathcal{S}_{0_4}^{r}\cup\mathcal{F}_{0_4}^{C}\cup\mathcal{S}_{0_4}^{a+}$ is smooth away from the line $\check{\ell}_{0_4}$.

ii. The manifold $\mathcal{S}_{0_4}$ has a folded structure; in particular, the branches $\mathcal{S}_{0_4}^{a-}$ and $\mathcal{S}_{0_4}^{r}$ are separated by the fold curve $\mathcal{F}_{0_4}^{A}$, while $\mathcal{S}_{0_4}^{r}$ and $\mathcal{S}_{0_4}^{a+}$ are separated by the fold curve $\mathcal{F}_{0_4}^{C}$.

iii. The branches $\mathcal{S}_{0_4}^{a-}$ and $\mathcal{S}_{0_4}^{a+}$ are attracting under the layer flow of Equation (50), while the branch $\mathcal{S}_{0_4}^{r}$ is repelling.

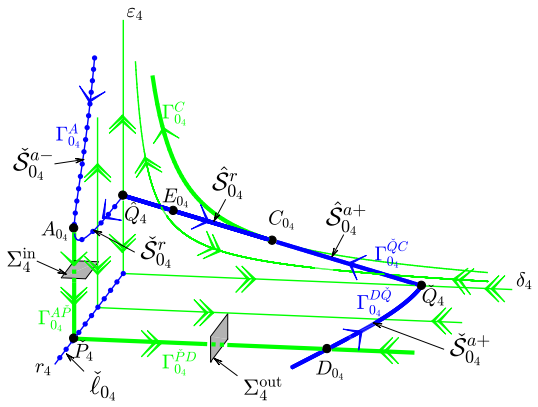

Fig. 11. Geometry in $\{\delta_4 = 0\}$, $\{\varepsilon_4 = 0\}$, and $\{r_4 = 0\}$, for $\kappa = 0$, in chart K_4: reduced flow (solid blue), layer dynamics (solid green), and equilibrium E_{0_4}.

iv. The restriction of $\mathcal{S}^r_{0_4}$ and $\mathcal{S}^{a+}_{0_4}$ to the invariant hyperplane $\{r_4 = 0\}$ corresponds to $\hat{\mathcal{S}}^r_{0_4}$ and $\hat{\mathcal{S}}^{a+}_{0_4}$, respectively. Correspondingly, the fold curve $\mathcal{F}^C_{0_4}$ intersects $\{r_4 = 0\}$ in the point C_{0_4}.

v. In the invariant hyperplane $\{\delta_4 = 0\}$, $\mathcal{S}^{a-}_{0_4}$ and $\mathcal{S}^r_{0_4}$ reduce to $\check{\mathcal{S}}^{a-}_{0_4}$ and $\check{\mathcal{S}}^r_{0_4}$, respectively. The fold curve $\mathcal{F}^A_{0_4}$ intersects $\{\delta_4 = 0\}$ in the point A_{0_4}.

vi. The restriction of $\mathcal{S}^{a+}_{0_4}$ to the invariant hyperplane $\{\varepsilon_4 = 0\}$ corresponds to $\check{\mathcal{S}}^{a+}_{0_4}$.

vii. The line $\check{\ell}_{0_4}$ consists of saddle-type equilibria for Equation (49), with 1-dimensional stable manifold in the hyperplane $\{\delta_4 = 0\}$ and 1-dimensional unstable manifold in the hyperplane $\{\varepsilon_4 = 0\}$.

Again, we define two sections Σ^{in}_4 and Σ^{out}_4 for the flow of Equation (49); here, the former is obtained as the image of the section Σ^{out}_3 from chart K_3 under the transformation $\mathcal{K}_{34}$ defined in Lemma 3, while the latter is the image of the section Σ^{in}_1 from chart K_1 in K_4 under the transformation

$$\mathcal{K}_{14} : (\rho_1, u_1, \varepsilon_1) \mapsto \big(r_4, \delta_4^2, \delta_4\varepsilon_4\big).$$

Hence, Σ^{in}_4 and Σ^{out}_4 can be represented as

$$\Sigma^{\text{in}}_4 := \left\{ \big(r_4, \delta_4, \sqrt{\Theta}\big) \,\middle|\, r_4 - \tfrac{1}{2\sqrt{\Theta b}} \in [r_*, r^*], \delta_4 \in [\delta_*, \delta^*] \right\} \quad \text{and} \tag{57a}$$

$$\Sigma^{\text{out}}_4 := \left\{ \big(r_4, \tfrac{\sqrt{\Theta}}{2}, \varepsilon_4\big) \,\middle|\, r_4 - \tfrac{1}{2\sqrt{\Theta b}} \in [r_*, r^*], \varepsilon_4 \in [\varepsilon_*, \varepsilon^*] \right\}, \tag{57b}$$

where the constants r_*, r^*, δ_*, δ^*, ε_*, and ε^* are again suitably chosen.

Remark 21. We emphasise that our blow-up of the non-hyperbolic line $\check{\ell}_{0_1}$ from chart K_1 to a cylinder has resulted in a gain of hyperbolicity; in particular, the line $\check{\ell}_{0_4}$ in K_4 is of saddle type, by item *vii* above.

To summarise, the segment $\Gamma^{A\check{P}}_{0_4}$ of the singular cycle is initiated close to the fold point A_{0_4} and is attracted to $\check{\mathcal{S}}^{a-}_{0_4}$, where it jumps forward along the fast flow to the point $\check{P}_4$; the orbit $\Gamma^{\check{P}D}_{0_4}$ then leaves along the unstable manifold thereof and is attracted by $\check{\mathcal{S}}^{a+}_{0_4}$, connecting to the point D_{0_4}. The orbit $\Gamma^{D\check{Q}}_{0_4}$ follows the slow flow on $\check{\mathcal{S}}^{a+}_{0_4}$ to the point $\check{Q}_4$ and continues as the orbit $\Gamma^{\check{Q}C}_{0_4}$ along the slow flow on $\hat{\mathcal{S}}^{a+}_{0_4}$ until it reaches the point C_{0_4}, where the orbit $\Gamma^C_{0_4}$ represents the jump back which is, however, not visible in chart K_4, but is discussed in K_3 already. (Clearly, the manifolds $\check{\mathcal{S}}^{a-}_{0_3}$, $\check{\mathcal{S}}^r_{0_3}$, $\hat{\mathcal{S}}^{a+}_{0_3}$, and $\hat{\mathcal{S}}^r_{0_3}$ defined in chart K_3 correspond to $\check{\mathcal{S}}^{a-}_{0_4}$, $\check{\mathcal{S}}^r_{0_4}$, $\hat{\mathcal{S}}^{a+}_{0_4}$, and $\hat{\mathcal{S}}^r_{0_4}$, respectively.) The geometry in the planes $\{\delta_4 = 0\}$, $\{\varepsilon_4 = 0\}$, and $\{r_4 = 0\}$ in chart K_4 is illustrated in Fig. 11.

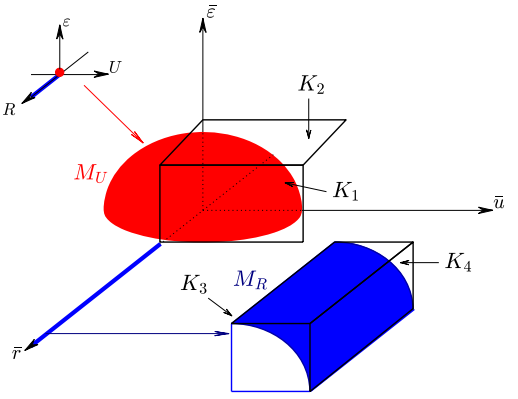

Fig. 12. The charts K_i $(i = 1, \dots, 4)$ in the blown-up space $\bar{M}_\kappa$.

4.7. Global geometry in blown-up space

We now summarise the global geometry of the blown-up space, which we denote as $\bar{M}_\kappa$, with $\kappa \in [0, \kappa_0]$. The above analysis implies that $\bar{M}_\kappa$ contains the sphere M_U and the cylinder M_R, which are obtained by the blow-up transformation in (24) at the origin Q in (R, U, ε)-space and the blow-up in (39) of the non-hyperbolic line $\check{\ell}_{0_1}$ in chart K_1 of the former, respectively; see Fig. 13. We recall that the vector field X_κ corresponding to Equation (6), which is defined on $\mathbb{R}^3$, induces a blown-up vector field $\bar{X}_\kappa$ on the blown-up space $\bar{M}_\kappa$; blow-up resolves the degeneracy of the critical manifold $\mathcal{S}_0$ – with κ as the singular perturbation parameter – at $\varepsilon = 0$. In particular, the equation $\varepsilon' = 0$ implies an invariant foliation of $\bar{M}_\kappa$ in ε, with the singular leaf defined by $\varepsilon = 0$ corresponding to the union of the sphere M_U, the cylinder M_R, and the plane $\{\bar{\varepsilon} = 0\}$. It follows that, for $\kappa = 0$, the restriction of $\bar{X}_0$ to that singular leaf represents the double singular limit of $(\kappa, \varepsilon) \to (0, 0)$, which has now been resolved in the blown-up space $\bar{M}_0$. The following results follow immediately from our discussion in Section 4; see also [13, Theorem 4.5].

Lemma 6. *The critical manifold of system (23), for $\kappa = 0$, in the blown-up space $\bar{M}_0$ is defined as*

$$\bar{\mathcal{S}}_0 = \bar{\mathcal{S}}_0^{a-} \cup \bar{\mathcal{F}}_0^A \cup \bar{\mathcal{S}}_0^r \cup \bar{\mathcal{F}}_0^C \cup \bar{\mathcal{S}}_0^{a+};$$

here, the branches $\bar{\mathcal{S}}_0^{a-}$ and $\bar{\mathcal{S}}_0^{a+}$ are attracting under the layer flow that is induced by Equation (8) after blow-up, while the branch $\bar{\mathcal{S}}_0^r$ is repelling. Moreover, $\bar{\mathcal{S}}_0^{a-}$ and $\bar{\mathcal{S}}_0^{a+}$ are separated by the fold curve $\bar{\mathcal{F}}_0^A$, while $\bar{\mathcal{S}}_0^r$ and $\bar{\mathcal{S}}_0^{a+}$ are separated by the fold curve $\bar{\mathcal{F}}_0^C$.

(We recall that, by Remark 13, any object $\Box_{\kappa\varepsilon}$ is written as $\bar{\Box}_\kappa$ after blow-up.)

Lemma 6 implies that a unique singular cycle $\bar{\Gamma}_{00}$ can now be defined in the blown-up space $\bar{M}_\kappa$ due to the improved transversality and hyperbolicity properties of the flow therein; for clarity, we label the corresponding persistent cycle in blown-up space by $\bar{\Gamma}_{\kappa\varepsilon}$ which, for $(\kappa, \varepsilon) \to (0, 0)$, yields the singular cycle $\bar{\Gamma}_{00}$.

Lemma 7. *The singular cycle $\bar{\Gamma}_{00}$ is defined by*

$$\bar{\Gamma}_{00} = \bar{\Gamma}_{00}^{A\check{P}} \cup \bar{\Gamma}_{00}^{\check{P}D} \cup \bar{\Gamma}_{00}^{D\check{Q}} \cup \bar{\Gamma}_{00}^{\check{Q}C} \cup \bar{\Gamma}_{00}^{CB} \cup \bar{\Gamma}_{00}^{B\hat{P}} \cup \bar{\Gamma}_{00}^{\hat{P}A}.$$

Here, the heteroclinic connection $\bar{\Gamma}_{00}^{A\check{P}}$ is located on the cylinder M_R and represents the fast jump from the point $\bar{A}_0$ to the point $\check{P} \in \bar{\mathcal{S}}_0^r$; the orbit $\bar{\Gamma}_{00}^{\check{P}D}$ lies in the plane $\{\bar{\varepsilon} = 0\}$, connecting $\check{P}$ to the point $\bar{D}_0 \in \bar{\mathcal{S}}_0^{a+}$. Finally, $\bar{\Gamma}_{00}^{D\check{Q}}$ represents the transition on $\bar{\mathcal{S}}_0^{a+}$ from $\bar{D}_0$ to the point $\check{Q}$. On the sphere M_U, the segment

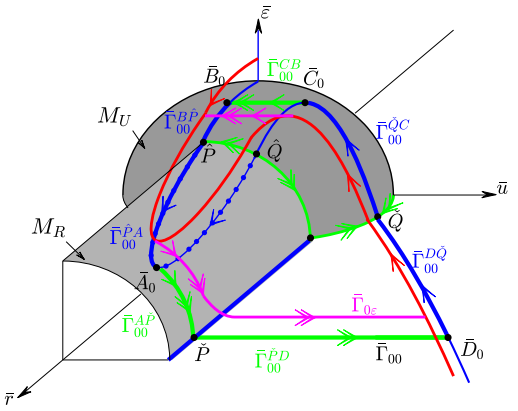

Fig. 13. Geometry of the blown-up space $\bar{M}_0$: singular cycle $\bar{\Gamma}_{00}$ (solid blue; solid green) and singular cycle $\bar{\Gamma}_{0\varepsilon}$ (solid red; solid pink).

$\bar{\Gamma}_{00}^{\check{Q}C}$ on $\bar{\mathcal{S}}_0^{a+}$ connects the point $\check{Q}$ to the fold point at $\bar{C}_0$; $\bar{\Gamma}_{00}^{CB}$ denotes the heteroclinic connection from $\bar{C}_0$ to the point $\bar{B}_0 \in \bar{\mathcal{S}}_0^{a-}$, followed by the orbit $\bar{\Gamma}_{00}^{B\hat{P}}$ from $\bar{B}_0$ to the point $\hat{P}$. The final segment $\bar{\Gamma}_{00}^{\hat{P}A}$ is located on the cylinder M_R, and denotes the connection on $\bar{\mathcal{S}}_0^{a-}$ from $\hat{P}$ to the fold point at $\bar{A}_0$.

An illustration of $\bar{\Gamma}_{00}$ can be found in Fig. 13; here, the reduced flow for $(\kappa, \varepsilon) = (0, 0)$ is shown in blue, as are the corresponding critical manifolds, while the layer dynamics is illustrated in green. We emphasise that chart K_2 is not required for our construction, strictly speaking, as the relevant portions of $\bar{\Gamma}_{00}$ can be obtained in either chart K_1 or K_3; recall Figs. 9 and 10, respectively.

Next, we have the following result on the persistence of $\bar{\Gamma}_{00}$, for ε positive and sufficiently small:

Lemma 8. *For $\varepsilon \in (0, \varepsilon_0]$, with ε_0 positive and sufficiently small, there exists a singular cycle $\bar{\Gamma}_{0\varepsilon}$ which follows the slow flow on $\bar{\mathcal{S}}_0^{a-}$ and $\bar{\mathcal{S}}_0^{a+}$, with jumps at the fold curves $\bar{\mathcal{F}}_0^A$ and $\bar{\mathcal{F}}_0^C$; that cycle limits on $\bar{\Gamma}_{00}$ as $\varepsilon \to 0$.*

The orbit $\bar{\Gamma}_{0\varepsilon}$ is again illustrated in Fig. 13; here, we emphasise that $\bar{\Gamma}_{0\varepsilon}$ is obtained as a perturbation off $\bar{\Gamma}_{00}$ for $\varepsilon \in (0, \varepsilon_0]$ and $\kappa = 0$. (The corresponding reduced flow is shown in red, while the layer dynamics is illustrated in pink.)

Remark 22. Intuitively, blow-up desingularises the limit as $\varepsilon \to 0$ in our definition of the critical manifold $\mathcal{S}_{0\varepsilon}$ for Equation (9), in that the non-uniform collapse of that manifold onto the degenerate manifold $\mathcal{S}_{00}$ has been prevented; in particular, the folded structure of $\mathcal{S}_{0\varepsilon}$ remains visible for $\varepsilon = 0$ after blow-up.

Finally, and in analogy to Theorem 4.6 in [13], we can conclude that, for $\kappa \in (0, \kappa_0]$, the blown-up vector field $\bar{X}_\kappa$ admits smooth slow manifolds $\bar{\mathcal{S}}_\kappa^{a-}$, $\bar{\mathcal{S}}_\kappa^{r}$, and $\bar{\mathcal{S}}_\kappa^{a+}$ away from the fold curves $\bar{\mathcal{F}}_0^A$ and $\bar{\mathcal{F}}_0^C$; in accordance with standard practice [23], we assume that these manifolds are extended beyond $\bar{\mathcal{F}}_0^A$ and $\bar{\mathcal{F}}_0^C$ by the flow corresponding to $\bar{X}_\kappa$.

5. Poincaré map and existence

To prove the persistence of the singular cycle $\bar{\Gamma}_{00}$ for κ and ε sufficiently small, we construct a Poincaré map in the neighbourhood of $\bar{\Gamma}_{00}$ which is obtained through the concatenation of three transition maps Π_i $(i = 1, 3, 4)$ between specific sections for the flow in the blown-up space $\bar{M}_\kappa$; see Fig. 14.

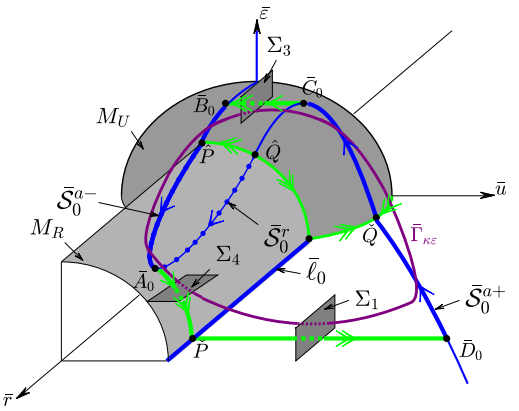

Fig. 14. Illustration of the Poincaré map Π: sections Σ_1, Σ_3, and Σ_4 (shaded dark grey); singular cycle $\bar{\Gamma}_{00}$ (solid blue; solid green); sample periodic orbit $\bar{\Gamma}_{\kappa\varepsilon}$ (solid purple).

i. The transition map $\Pi_1 : \Sigma_1 \to \Sigma_3$ is initialised in the section Σ_1; the corresponding flow is attracted to the slow manifold $\bar{\mathcal{S}}_\kappa^{a+}$, which it follows up to the non-hyperbolic fold curve $\bar{\mathcal{F}}_0^C$, where it jumps, remaining close to the heteroclinic connection $\bar{\Gamma}_{00}^{CB}$ to reach a section Σ_3.
ii. The transition map $\Pi_3 : \Sigma_3 \to \Sigma_4$ is initialised in the section Σ_3; the corresponding flow is attracted to the slow manifold $\bar{\mathcal{S}}_\kappa^{a-}$, which it follows up to the non-hyperbolic fold curve $\bar{\mathcal{F}}_0^A$. It then jumps, remaining close to the heteroclinic connection $\bar{\Gamma}_{00}^{A\check{P}}$, to reach a section Σ_4.
iii. The transition map $\Pi_4 : \Sigma_4 \to \Sigma_1$ is initialised in the section Σ_4; the corresponding flow then remains close to the heteroclinic connection $\bar{\Gamma}_{00}^{A\check{P}}$, passing near the hyperbolic line $\bar{\ell}_0$ and the singular heteroclinic $\bar{\Gamma}_{00}^{\check{P}D}$ to reach a section Σ_1.

The Poincaré map $\Pi : \Sigma_1 \to \Sigma_1$, which is a global return map, is now defined as the composition $\Pi = \Pi_4 \circ \Pi_3 \circ \Pi_1$. Here, we note that the maps Π_i $(i = 1, 3, 4)$ are constructed in charts K_i, respectively; details can be found in the following subsections.

Remark 23. The sections Σ_1, Σ_3, and Σ_4 are defined to be transversal to the heteroclinic orbits $\bar{\Gamma}_{00}^{\check{P}D}$, $\bar{\Gamma}_{00}^{CB}$, and $\bar{\Gamma}_{00}^{A\check{P}}$, respectively; see again Fig. 14.

5.1. Transition map Π_1

The transition map Π_1 is constructed in chart K_1 as a mapping between the sections Σ_1 and Σ_3, which correspond to Σ_1^{in} and Σ_1^{out}, respectively; recall Equation (38). We note that, since $\varepsilon = \rho_1^2 \varepsilon_1$ in K_1, invariant leaves of the form $\{\varepsilon \equiv \text{constant}\}$ satisfy $\varepsilon_1 \approx 4\Theta\tilde{b}\varepsilon$ in Σ_1^{in} and $\rho_1 \approx \frac{2}{\sqrt{\Theta}}\sqrt{\varepsilon}$ in Σ_1^{out}.

Lemma 9. *For $(\kappa, \varepsilon) \in (0, \kappa_0] \times (0, \varepsilon_0]$, with κ_0 and ε_0 positive and sufficiently small, the transition map Π_1 is well-defined. Moreover, the restriction of Π_1 to the leaf $\{\varepsilon \equiv \text{constant}\}$ is a contraction (in ρ_1) with contraction rate $\mathcal{O}(\mathrm{e}^{-\nu/\kappa})$, where ν is a positive constant.*

Proof. The passage past a regular fold point is studied in detail in [14]; in particular, it follows from the analysis therein that orbits initiated in Σ_1^{in} are attracted by the extended slow manifold $\bar{\mathcal{S}}_\kappa^{a+}$ at a contraction rate of the order $\mathcal{O}(\mathrm{e}^{-\nu/\kappa})$, while the distance between the intersection of that extended manifold with Σ_1^{out} and the singular cycle $\bar{\Gamma}_{00}$ is of the order $\mathcal{O}(\kappa^{2/3})$. □

Remark 24. While our approximation of the transition map Π_1 is performed in chart K_1, the dynamics in that chart can also be recovered in regime $\mathcal{R}_2$. Hence, the results of [14] on passage past a singularly

perturbed planar fold can be applied to Equation (18). For a more detailed analysis of chart K_1, we refer to [23], where general folds in $\mathbb{R}^3$ are studied. Finally, we remark that passage past the point $\breve{Q}_1$ can be described in terms of well-adapted normal forms that are derived in [1].

5.2. Transition map Π_3

The transition map Π_3 is constructed in chart K_3 as a mapping between the sections Σ_3 and Σ_4. Here, we recall that these sections correspond to Σ_3^{in} and Σ_3^{out}, respectively; cf. Equation (48). Due to $\varepsilon = r_3^2\delta_3$ in K_3, leaves with $\{\varepsilon \equiv \text{constant}\}$ satisfy $r_3 \approx \sqrt{\frac{4}{\Theta}\varepsilon}$ in Σ_3^{in} and $\delta_3 \approx 4\Theta\tilde{b}\varepsilon$ in Σ_3^{out}.

We have the following result, the proof of which is analogous to that of Lemma 9:

Lemma 10. *For $(\kappa,\varepsilon) \in (0,\kappa_0] \times (0,\varepsilon_0]$, with κ_0 and ε_0 positive and sufficiently small, the transition map Π_3 is well-defined. Moreover, the restriction of Π_3 to the leaf $\{\varepsilon \equiv \text{constant}\}$ is a contraction (in r_3) with contraction rate $\mathcal{O}(\mathrm{e}^{-\nu/\kappa})$, where ν is a positive constant.*

Remark 25. Again, the map Π_3 can alternatively be approximated in regime $\mathcal{R}_1$, i.e., by reference to Equation (14), to which the results of [14] apply. A more detailed analysis of chart K_3 can be based on [23].

5.3. Transition map Π_4

The transition map Π_4 is constructed in chart K_4 as a mapping between the sections Σ_4 and Σ_1 which correspond to Σ_4^{in} and Σ_4^{out}, respectively, as defined in Equation (57).

Lemma 11. *For $(\kappa,\varepsilon) \in (0,\kappa_0] \times (0,\varepsilon_0]$, with κ_0 and ε_0 positive and sufficiently small, the transition map $\Pi_4 : \Sigma_4 \to \Sigma_1,\ (r_4^{\text{in}}, \delta_4^{\text{in}}, \sqrt{\Theta}) \mapsto \left(r_4^{\text{out}}, \frac{\sqrt{\Theta}}{2}, \varepsilon_4^{\text{out}}\right)$ is well-defined; here, $\delta_4^{\text{in}} \approx 4\sqrt{\Theta}\tilde{b}\varepsilon$ and $\varepsilon_4^{\text{out}} \approx 8\sqrt{\Theta}\tilde{b}\varepsilon$. In particular, as the restriction of Π_4 to a leaf $\{\varepsilon \equiv \text{constant}\}$ satisfies*

$$r_4^{\text{out}} = r_4^{\text{in}} + \mathcal{O}(\kappa)$$

with $r_4^{\text{in}} \approx \frac{1}{2\sqrt{\Theta\tilde{b}}}$, the map Π_4 is at mostly weakly expanding.

Proof. Recall the governing equations in chart K_4, as given in Equation (49), as well as the definition of $F_4(r_4,\delta_4,\varepsilon_4)$ therein; dividing out the factor $\frac{1}{2}\left\{\tilde{b}r_4^2\varepsilon_4^2(\delta_4+\varepsilon_4)^2 + \Theta - \left[(\delta_4+\varepsilon_4)^2 + \Lambda r_4^2\delta_4^2\right]\right\}$ from the right-hand sides in (49) and factoring out $\delta_4^{\frac{1}{2}}$ from F_4, we obtain the new system

$$r_4' = \kappa r_4\delta_4^{\frac{1}{2}}\tilde{F}_4(r_4,\delta_4,\varepsilon_4), \tag{58a}$$

$$\delta_4' = \delta_4 - \kappa\delta_4^{\frac{3}{2}}\tilde{F}_4(r_4,\delta_4,\varepsilon_4), \tag{58b}$$

$$\varepsilon_4' = -\varepsilon_4 - \kappa\delta_4^{\frac{1}{2}}\varepsilon_4\tilde{F}_4(r_4,\delta_4,\varepsilon_4), \tag{58c}$$

where $\tilde{F}_4(r_4,\delta_4,\varepsilon_4)$ is smooth and $\mathcal{O}(1)$. Equation (58) is again a slow-fast system in standard form; considering the layer problem

$$\begin{aligned} r_4' &= 0,\\ \delta_4' &= \delta_4,\\ \varepsilon_4' &= -\varepsilon_4, \end{aligned}$$

we can estimate the transition time T_4 in $\{\varepsilon \equiv \text{constant}\}$ under Π_4: since $\delta_4 \approx 4\sqrt{\Theta}\,\tilde{b}\varepsilon$ in Σ_4^{in} and $\varepsilon_4 \approx 8\sqrt{\Theta}\,\tilde{b}\varepsilon$ in Σ_4^{out} due to $\varepsilon = r_4^2\delta_4\varepsilon_4$ in chart K_4, it follows that $T_4 = \mathcal{O}(-\ln\varepsilon)$. Finally, since $r_4\delta_4^{\frac{1}{2}} = \sqrt{\frac{\varepsilon}{\varepsilon_4}}$ and $\varepsilon_4 \approx \sqrt{\Theta}\mathrm{e}^{-t}$, we may write (58a) as $r_4' = \kappa\sqrt{\varepsilon}\mathrm{e}^{t/2}\cdot\mathcal{O}(1)$, from which the statement of the lemma follows. □

5.4. Proof of Theorem 1

To conclude the proof of Theorem 1, we combine the above asymptotics of the transition maps Π_i $(i = 1, 3, 4)$ into the Poincaré map Π, which yields

Theorem 2. *For $\varepsilon \in (0, \varepsilon_0]$, with ε_0 positive and sufficiently small, there exists $\kappa_0 = \kappa_0(\varepsilon_0)$ such that the blown-up vector field $\bar{X}_\kappa$ admits a unique family of attracting periodic orbits $\bar{\Gamma}_{\kappa\varepsilon}$ for $\kappa \in (0, \kappa_0]$. That family tends to $\bar{\Gamma}_{0\varepsilon}$ as $\kappa \to 0$ uniformly for $\varepsilon \in (0, \varepsilon_0]$, and converges to the singular cycle $\bar{\Gamma}_{00}$ as $(\kappa, \varepsilon) \to (0, 0)$.*

Proof. The proof follows from a combination of Lemmas 9, 10, and 11, in conjunction with the contraction mapping theorem. Specifically, since $\rho_1 = R = r_3$, the restriction of the maps Π_1 and Π_3 to leaves with $\{\varepsilon \equiv \text{constant}\}$ is contracting in R, while Π_4 is at most weakly expanding in $R(= r_4)$. □

An indicative illustration of the orbit $\bar{\Gamma}_{\kappa\varepsilon}$, for (κ, ε) positive and fixed, can be found in Fig. 14.
Theorem 1 is a direct consequence of Theorem 2 after blow-down.

6. Discussion

In the present article, we have performed a geometric analysis of a singularly perturbed two-variable model for a cyclic AMP (cAMP) signalling system. The model is obtained from a scaling of the three-variable Martiel-Goldbeter model [16] which is due to Lițcanu and Velázquez [15]. The planar system resulting from a quasi-steady-state assumption, Equation (5), represents a two-parameter singular perturbation problem; the presence of two parameters κ and ε in the model manifests in a highly degenerate, and non-standard, singular limit as $(\kappa, \varepsilon) \to (0, 0)$ which is resolved via a combination of geometric singular perturbation theory and the desingularisation technique known as blow-up. In particular, our approach allows us to describe in detail the global geometry of the model in the limit as both singular perturbation parameters tend to zero; the underlying critical manifold, consisting of one non-hyperbolic line in the "inner" region and one normally hyperbolic curve in the "outer" region which meet at a degenerate equilibrium at the origin, is desingularised in the process. Our resolution of those degeneracies is motivated by a similar study of the Goldbeter-Lefever model by Kosiuk and Szmolyan [13] and permits us to construct a family of periodic (relaxation-type) cycles for Equation (59), thus shedding light on a novel singular perturbation problem and improving our understanding of the corresponding oscillatory dynamics.

In future, we intend to extend our analysis to the three-variable reaction-diffusion system [15]

$$R_\tau(\tilde{x}, \tau) = \kappa(U + \mathcal{P}\varepsilon)\frac{\mu(U+\varepsilon) - (U + d\varepsilon)R}{(U + \frac{\varepsilon}{c})(U+\varepsilon)}, \tag{59a}$$

$$W_\tau(\tilde{x}, \tau) = \frac{b\varepsilon(U+\varepsilon)^2 + \Theta R^2U^2}{(U+\varepsilon)^2 + \Lambda R^2U^2} - W, \tag{59b}$$

$$U_\tau(\tilde{x}, \tau) = U_{\tilde{x}\tilde{x}} + \Gamma(W - U), \tag{59c}$$

which incorporates an extracellular cAMP diffusion term, as introduced in [25]. Correspondingly, R, W, and U are functions of both space $\tilde{x}$ and time τ, with $x = \sqrt{\frac{D}{k_i + k_t}}\tilde{x}$; cf. again Table 1. The main result of [15] is a proof for the existence of travelling pulse solutions to (59) in one spatial dimension on the basis

of singular perturbation theory, under the assumption that the parameters κ and ε are small; moreover, asymptotic formulae are derived for these pulse solutions in a number of relevant scaling regimes.

We expect that a geometric construction of these solutions can be based on the framework established here, in the context of our simplified two-variable Equation (5). However, in preliminary work, we have not managed to find a scaling for regime $\mathcal{R}_1$ that allows us to establish an overlap with $\mathcal{R}_3$; recall our discussion in Section 4.4. That failing is mirrored by the fact that a key non-linear eigenvalue problem in [15, Section 4.1.2] has to be solved numerically to allow for the calculation of the unique velocity of travelling pulses. Hence, we believe that further investigation is warranted.

Acknowledgments

The research of Z. Miao was funded in part by WWTF (Vienna Science and Technology Fund) Grant MA 14-049. The research of P. Szmolyan was funded by WWTF Grant MA 14-049.

References

[1] P. Bonckaert, P. De Maesschalck, F. Dumortier, Well adapted normal linearization in singular perturbation problems, J. Dynam. Differential Equations 23 (1) (mar 2011) 115–139.
[2] E. Brieskorn, H. Knörrer, Plane Algebraic Curves: Translated by John Stillwell, Birkhäuser Verlag, Basel, 1986.
[3] F. Dumortier, Techniques in the theory of local bifurcations: blow-up, normal forms, nilpotent bifurcations, singular perturbations, in: Bifurcations and Periodic Orbits of Vector Fields, Springer, Dordrecht, 1993, pp. 19–73.
[4] N. Fenichel, Geometric singular perturbation theory for ordinary differential equations, J. Differential Equations 31 (1) (jan 1979) 53–98.
[5] G. Gerisch, B. Hess, Cyclic-AMP-controlled oscillations in suspended dictyostelium cells: their relation to morphogenetic cell interactions, Proc. Nat. Acad. Sci. 71 (5) (may 1974) 2118–2122.
[6] G. Gerisch, D. Malchow, Cyclic AMP receptors and the control of cell aggregation in dictyostelium, Adv. Cycl. Nucleotide Res. 7 (1976) 49–68.
[7] G. Gerisch, D. Malchow, W. Roos, U. Wick, Oscillations of cyclic nucleotide concentrations in relation to the excitability of dictyostelium cells, J. Exp. Biol. 81 (1979) 33–47.
[8] G. Gerisch, U. Wick, Intracellular oscillations and release of cyclic AMP from dictyostelium cells, Biochem. Biophys. Res. Commun. 65 (1) (jul 1975) 364–370.
[9] A. Goldbeter, L.A. Segel, Unified mechanism for relay and oscillation of cyclic AMP in dictyostelium discoideum, Proc. Natl. Acad. Sci. 74 (4) (apr 1977) 1543–1547.
[10] A. Goldbeter, L.A. Segel, Control of developmental transitions in the cyclic AMP signalling system of dictyostelium discoideum, Differentiation 17 (1–3) (dec 1980) 127–135.
[11] G. Hek, Geometric singular perturbation theory in biological practice, J. Math. Biol. 60 (3) (2010) 347–386.
[12] C.K.R.T. Jones, Geometric singular perturbation theory, in: Dynamical Systems: Lectures Given at the 2nd Session of the Centro Internazionale Matematico Estivo Held in Montecatini Terme, Italy, June 13–22, 1994, Springer, Berlin Heidelberg, 1995, pp. 44–118.
[13] I. Kosiuk, P. Szmolyan, Scaling in singular perturbation problems: blowing up a relaxation oscillator, SIAM J. Appl. Dyn. Syst. 10 (4) (jan 2011) 1307–1343.
[14] M. Krupa, P. Szmolyan, Extending geometric singular perturbation theory to nonhyperbolic points—fold and canard points in two dimensions, SIAM J. Math. Anal. 33 (2) (jan 2001) 286–314.
[15] G. Liţcanu, J.J.L. Velázquez, Singular perturbation analysis of cAMP signalling in dictyostelium discoideum aggregates, J. Math. Biol. 52 (5) (mar 2006) 682–718.
[16] J.L. Martiel, A. Goldbeter, A model based on receptor desensitization for cyclic AMP signaling in dictyostelium cells, Biophys. J. 52 (5) (nov 1987) 807–828.
[17] E.F. Mishchenko, N.Kh. Rozov, Differential Equations with Small Parameters and Relaxation Oscillations: Translated by F.M.C. Goodspeed, Plenum Press, New York, 1980.
[18] W. Roos, G. Gerisch, Receptor-mediated adenylate cyclase activation in Dictyostelium discoideum, FEBS Lett. 68 (2) (oct 1976) 170–172.
[19] W. Roos, V. Nanjundiah, D. Malchow, G. Gerisch, Amplification of cyclic-AMP signals in aggregating cells of Dictyostelium discoideum, FEBS Lett. 53 (2) (may 1975) 139–142.
[20] W. Roos, C. Scheidegger, G. Gerisch, Adenylate cyclase activity oscillations as signals for cell aggregation in dictyostelium discoideum, Nature 266 (5599) (mar 1977) 259–261.
[21] L. Segel, A. Goldbeter, Scaling in biochemical kinetics: dissection of a relaxation oscillator, J. Math. Biol. 32 (2) (jan 1994) 147–160.
[22] B.M. Shaffer, Secretion of cyclic AMP induced by cyclic AMP in the cellular slime mould dictyostelium discoideum, Nature 255 (5509) (jun 1975) 549–552.
[23] P. Szmolyan, M. Wechselberger, Relaxation oscillations in $\mathbb{R}^3$, J. Differential Equations 200 (1) (jun 2004) 69–104.

[24] A. Theibert, Cyclic 3', 5'-AMP relay in dictyostelium discoideum: adaptation is independent of activation of adenylate cyclase, J. Cell Biol. 97 (1) (jul 1983) 173–177.
[25] J.J. Tyson, K.A. Alexander, V.S. Manoranjan, J.D. Murray, Spiral waves of cyclic AMP in a model of slime mold aggregation, Phys. D, Nonlinear Phenom. 34 (1–2) (jan 1989) 193–207.